The Impact of Printing Orientation on The Tensile Properties of Parts Printed by Fused Deposition Modelling

Nhu Tran

Degree Thesis

Materials Processing Technology

2019

DEGREE THESIS	
Arcada	
Degree Programme:	Materials Processing Technology 2016
Identification number:	19997
Author:	Luc Phuong Nhu Tran
Title:	
Supervisor (Arcada):	Mathew Vihtonen
Commissioned by:	

Abstract:
This thesis work aims to study the relation between the tensile properties and print orientation of a PLA product produced by FDM printing process. The testing methods include tensile tests, analytical calculation and computational simulation. Testing specimens were printed based on ISO 527-2 standard. There are totally 11 types of models with diverse print settings. Tensile tests were conducted on samples printed in 3 fundamental orientations (flat, on-edge and upright), along with layer height (0.1, 0.2, 0.5 mm) and infill density (10%, 50%, 95%). The experiment examines the main tensile properties: elastic modulus, ultimate tensile strength, and strain. Optical microscopy was used for examining samples' surface microstructure.

The principal stress measured in COMSOL software is 17.64% higher and 16% lower than the ones derived from the Mohr's circle and the stress concentration method, respectively. Experimental results show that the upright printed specimens possessed the lowest strength among three orientations and the strength difference for many print parameters between the flat and on-edge position is slightly small, ranging from 0.34% to 4.3%. However, in the case when the layer height was set at 0.5 mm, this difference has risen up to 37%. Moreover, it was found that the tensile strength was considerably enhanced when the infill density was set at 95%. Although process parameters were proved to have an effect on the overall strength of the manufactured part, there are other factors which could be applied to optimize the material properties.

Keywords:	3D Printing, FDM, PLA, Tensile Properties, Optical Microscopy
Number of pages:	66
Language:	English
Date of acceptance:	

CONTENTS

Figures

Tables

List of Symbols

σ	Nominal stress
ε	Nominal strain
E	Elastic modulus
τ	Shear stress
σ_1, σ_2	Maximum and minimum normal stress
ρ	Density
ν	Possion's ratio
K	Stress concentration factor

1 INTRODUCTION

1.1 Background

The use of 3D printing in rapid prototyping and production has increased significantly in recent years. Current 3D printers can produce complex geometries or a whole assembly with high accuracy in a short period of time, which made 3D printing very popular in aerospace, automotive, electronic, and healthcare, etc. [1]

Several researches have been taken to enhance the technology, develop new printing materials, or to reduce printing time, and material waste. However, the most fundamental factors controlling the material properties of a printed part are printing parameters. Many studied about this subject were conducted but the results varied greatly according to the type of material and printer used. Ayrilmis, N et al. [2] investigated the effect of layer thickness on the mechanical properties of 3D printed wood/PLA composites. Similar research on 3D printed ABS was carried out by Shubham, P et al. [3]. Yao, T et al. [4] formed a method to estimate the tensile strength of 3D printed PLA in several orientations ranging from 0° to 90°.

This thesis investigates the tensile properties of fused deposition modelling (FDM) specimen 3D printed with different parameters, focusing particularly on printing orientation. The printing material is polylactic acid (PLA). PLA is quite brittle in nature, making it more prone to break under stress, compared with the high strength of ABS, another common FDM printing filament. But due to its biodegradable and environmental-friendly characteristics, PLA is highly favoured in producing sustainable products. Then, knowing what type of setting can result in higher mechanical strength is extremely important in production, especially in making a functional object or device. The final outcomes will give some proposals for possible choices of parameters that the users can choose to improve the product's mechanical strength.

1.2 Objectives

The thesis has the following five objectives:

- Design the ISO 527-2 standard test piece in SolidWorks.
- 3D print and test samples using several printing settings.
- Analyse tensile testing results using mathematical calculation, computational simulation and data from practical tests.
- Observe the surface's microstructure with an optical microscope by mounting the specimens on the stage holder.
- Compare the mechanical properties (elastic modulus, tensile strength, elongation at break) among different types of samples.

1.3 Relevance of the problem

Studying this topic at the moment is very relevant since there are a number of researches which have been conducted to develop new printing materials and enhance the technology mechanism. Multiple benefits can be obtained from this study, including plastic waste reduction, time and material saving, or better surface finish and quality.

1.4 Relationship to existing knowledge

This thesis is conducted on the basis of various courses that have been taught at Arcada. Fused deposition modelling (FDM) is one of the most popular techniques among 3D printing hobbyists as the use of FDM printers does not require users to have professional skills to operate it. However, it is not easy to control the physical properties of the printed part, and their quality can vary among different types of printer. As a result, there are several factors needed to be taken into account when designing an object such as its size, the filament used, the build orientation or possible degradation while printing, etc. This

study addresses the connection between mechanical properties and printing parameters of a printed part as well.

2 LITERATURE REVIEW

2.1 Additive Manufacturing

Since the first development of 3D printing in the early 1980s, this technology has become a revolution in the manufacturing of products. 3D printing and rapid prototyping belong to the same category with additive manufacturing, in which a physical solid object is formed by accumulating layers of material according to a computational file [10]. The materials utilized varies from plastic, metal or even human tissues. In the initial period when 3D printing had just been invented, it was usually referred to rapid prototyping, a process of quickly fabricating a model by additive manufacturing technology before mass-producing in conventional processes. The consistent advancement of 3D printing has turned this technology into a hobby for numerous designers, researchers, inventors, etc. who freely design and create their own products. 3D printing in the early 1980s was restricted to certain applications and designs, but its great value and potential to the manufacturing industry has never been denied. As technicians continuously tested and troubleshot any issues existing in the technology, 3D printing has made a great leap forward with its achievements over the past years. 3D printing now has the advantage of high productivity and flexibility, shorter production time, higher accuracy, material waste reduction, overall cost reduction, better product quality, and producing lightweight products [4].

The first additive manufacturing machine dated back to 1981, when Hideo Kodama of Nagoya Municipal Industrial Research Institute introduced a system fabricating a solid model layer upon layer using photopolymers [5]. In 1984, Charles Hull the founder of 3D Systems, initiated the era of 3D printing with the invention of stereolithography (SLA), a technique that utilized ultraviolet light on the photopolymer for the purpose of building the desired objects. He also created the stereolithography STL file format in order to be interpreted by any 3D printers. Hull has made the 3D printing history with his great contribution, and the common use of this file format nowadays in various additive manufacturing processes has proven it. In 1986, Carl Deckard and Joe Beaman built the first selected laser sintering (SLS) printer, being also the first printer that could use metal to prototype models. The next new 3D printing process was created by Scott Crump, the

founder of Stratasys, in 1989. He was both the creator of fused deposition modelling (FDM) process and the utilization of ABS (acrylonitrile butadiene styrene) filament in an FDM printer. Stratasys together with 3D Systems becomes the largest 3D printing firms in the world. The growth of FDM technology has gained popularity in the majority of 3D printing users since its first appearance. Furthermore, the Massachusetts Institute of Technology (MIT) firstly applied the term 3D printing in the early 1990s when inkjet 3D printing technique was developed [4]. With the development of all 3D printing processes, the technology has never ceased to progress. Several software and printers with the most advanced functions have been created. The 21st century marked a new era of the additive manufacturing technology. 3D printer now is not just a prototyping machine, but it has the capability in fabricating human organ from the patient's tissues, body parts and printing itself. The self-replicating printer idea was originated from the RepRap Project of Adrian Bowyer in 2005, followed by the release of the Darwin printer in 2008, which works upon the same principle [5].

The RepRap project had initiated the constant development of consumer 3D printers. In the first 20 years since the development of rapid prototyping technology, all the printers whose cost were more than $100 000, were aimed for the industrial and commercial markets [6]. The high price together with the appearance of several business manufacturing affordable printers have turned the marketplace from industrial to consumer. The first consumer 3D printing machine was sold in 2008. In 2013 alone, 140 425 low-cost printers have been purchased, compared with 66 700 printers of the industrial sector [7]. The average price of an industry and personal printer is $73 800 and $1208 respectively, emphasizing the need to produce more simple and inexpensive 3D printing units.

Though there are various types of printing process today, the overall additive manufacturing process includes the same procedure, which is designing, file format conversion and the printer settings modification, printing, and lastly post processing. The first step is to produce a computer-aided-design (CAD) model using CAD software (AutoCAD, SolidWorks). When designing a part, one must consider every issues and limitations (application, printer capability) that can possibly occur during the printing in order to prevent unexpected failures. Then, the CAD file is converted to STL file and the printing parameters such as infill, layer height, printing speed, or cross-section pattern etc. are adjusted to suit the user's need. Before sending the file to print, a slicer program slices the digital

model into several layers across its cross section. Afterwards, the user sends the file to a 3D printer and only needs to press the start button and the whole process is automatically done until the object is completely built. However, the printing process can be stopped when there is not enough material, or the filament gets jammed, or when there is a fault in the machine. When the printing is finished, carefully take the physical model out. Some complicated-shaped parts require professional skill and equipment to remove both from the built plate and the support material. Lastly, the post process for the printed parts is one of the most essential steps before sending the products for use. The treatment mitigates the surface roughness and porosity, as well as enhance the microstructure [8]. There is a variety of methods that we can choose from: sanding, polishing, colouring stage, UV curing, or stress relieving for metal parts [9].

Additive manufacturing consists of a variety of processes from which manufacturers or individuals can select depending on application, appearance, function, quality, manufacturing cost etc. of the products. Different types of technique produce different types of product with different prices and time. A hobbyist can be satisfied with printing objects with an FDM printer because the costs for both the printer and filaments are reasonable. On the other hand, industrial-level products demand higher investment for a high-end machine which costs up to 30,000 USD (26,900 EUR) and other materials like resins, metal powders, ceramics and composites [10]. All the current commercial additive manufacturing processes fall into 7 main categories, with a few highlighted techniques are listed below: [11]

- Vat photopolymerization (Stereolithography);
- Powder bed fusion (Selective laser sintering);
- Material extrusion (Fused deposition modelling);
- Material jetting;
- Binder jetting;
- Direct energy deposition (Laser engineered net shape).

In the 1980s, 3D printing was still in its infancy, the 3D printers had low quality and accuracy, the materials used were limited. Those are the reasons why this technology was only applicable in some restricted fields like rapid prototyping. After almost 40 years, the technology has developed so rapidly that it is utilized in a wide range of applications, with product development, manufacturing, construction, medical application being the most crucial ones. The increase in materials available for additive manufacturing and the low-cost printers are the factors that facilitate the construction of buildings or bridges totally by this technology [12]. In the medical section, researchers and engineers have successfully printed tissues and organs from living cells, and prosthetics that fit its patient's body part [12]. Dvir, T et al. [13] has successfully 3D printed a tiny heart from stem cells converted from patients' fat cells. It consists of every parts of a normal heart like cells, blood vessels, chambers, etc. but the compatibility of the printed organ with human body still requires further examination. Manufacturers also favour the use of 3D printing, especially the FDM technique, in producing castable metal patterns due to the inexpensive price to make the tooling and the ability to fabricate a large-sized part compared to conventional process like CNC [14]. Moreover, the 3D printing technology is widely employed in the automotive and aerospace industry [10].

Figure 1. *A 3D printed house in Austin, Texas* [15]

Although prototyping still dominates the functional sector of 3D printing, more and more investments have been increased in other areas like art, education, fashion, hobby [1]. Individuals have a wide variety of choices choosing the most appropriate machine provided by numerous 3D printing companies. Today various schools have added the 3D

printing course in their curriculum, which teaches students to design and create their own products. Furthermore, 3D printers can be easily found in many local libraries. Jewellery and fashion industry are also interested in this technology. Customers can order unique or customized jewelleries, clothing from many websites that design and 3D print ornaments [12]. In addition, several researches regarding 3D food printing have been carried on in order to investigate the practicability of this application [50]. This fascinating idea is going to be a new potential application of additive manufacturing in the future.

2.1.1 Fused Deposition Modelling (FDM) Technique

Out of all 3D printing technologies, Fused Deposition Modelling (FDM), also called Fused Filament Fabrication (FFF), is the most popular technique which works on a solid-based 3D printing system. An FDM printer is inexpensive compared to other technologies and its process is easy to operate. This has made the technology common to the beginners as there are no skills required to run the machine, and this basic printer is widely utilized by schools, libraries or offices.

As mentioned before, this method starts by creating a computer graphical model from a CAD program then sending it to an FDM-designed slicer program. The program splits the model into several layers, and with the adjustment of printer setting parameters, the data of the model is saved and imported to the FDM printer.

The basic principle to fabricate a physical part of the FDM process is by extruding the melted plastic through the head of the heated printer nozzle layer-by-layer until the object is completed [51]. The thermoplastic materials used generally are in the form of a filament, and they are connected to the machine extruder where they will transform from a solid state to a melted state while printing. Most of the FDM printers can only print one type of material and colour at once, but multi-materials 3D printers have already been created and there is no doubt they will be more available in the future.

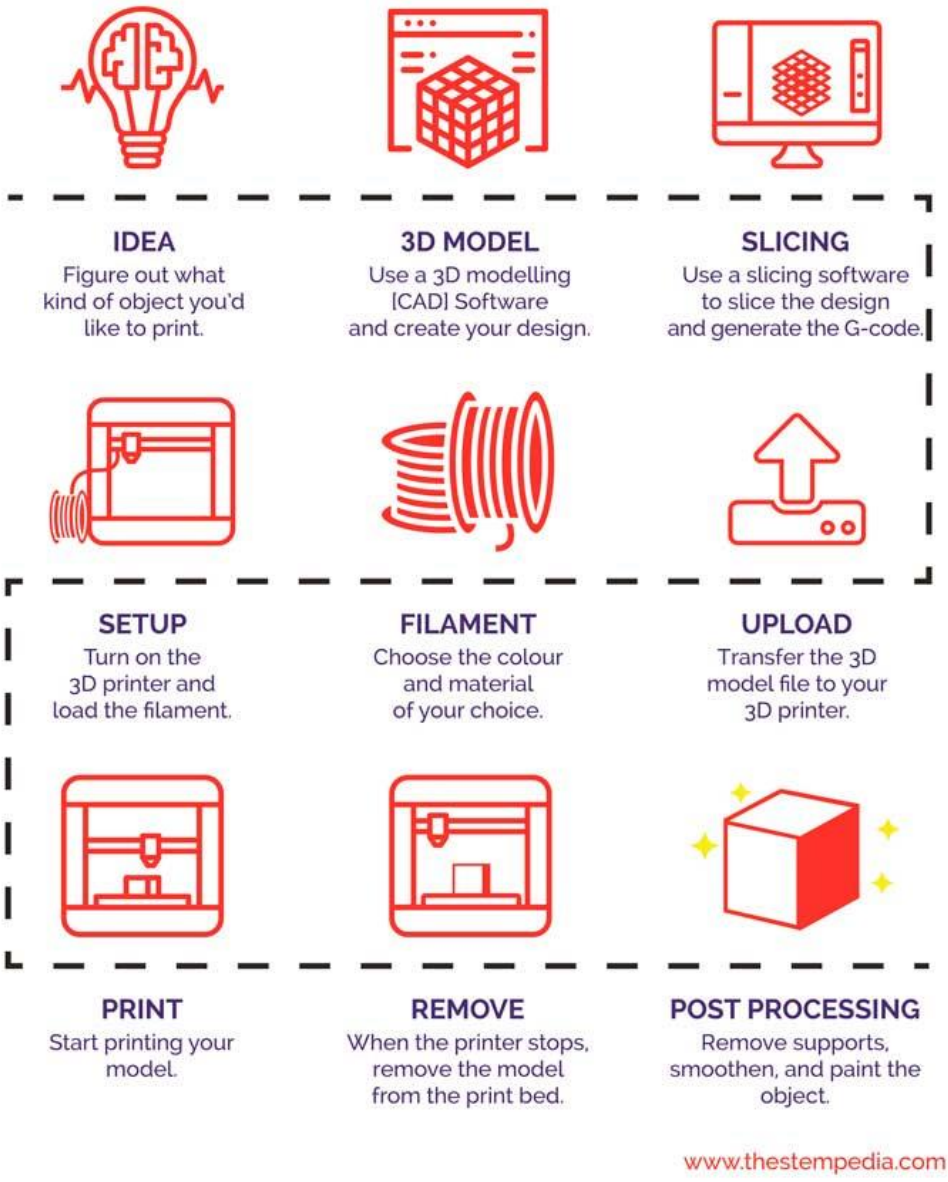

Figure 2. *The overview of the FDM process* [16]

In the printing process, when the nozzle and the printing bed has reached the set temperature, the filament is pushed down by the extruder's gear, melted and is extruded out from the nozzle at the determined position. Most of the filaments have a typical diameter of 1.75 mm, and 0.2 mm or 0.4 mm for the nozzle's diameter [17]. Both the nozzle head and the build platform move in the XYZ coordinate so either the platform goes down or the nozzle goes up after one finished layer in order to extrude the next layer [18]. Each layer is first printed at the outermost contour and then filled in the inside. When a layer is deposited, it cools down, solidifies and fuses with the next layer, which is the way a solid model formed. Finally, the finished part is taken out from the printing bed simply by hand

or a scrapper and post processing might be done as the layer lines can easily be seen on the FDM printed object. A number of post processing techniques include sanding, polishing, vapor smoothing, dipping, priming and printing, epoxy coating, etc [19].

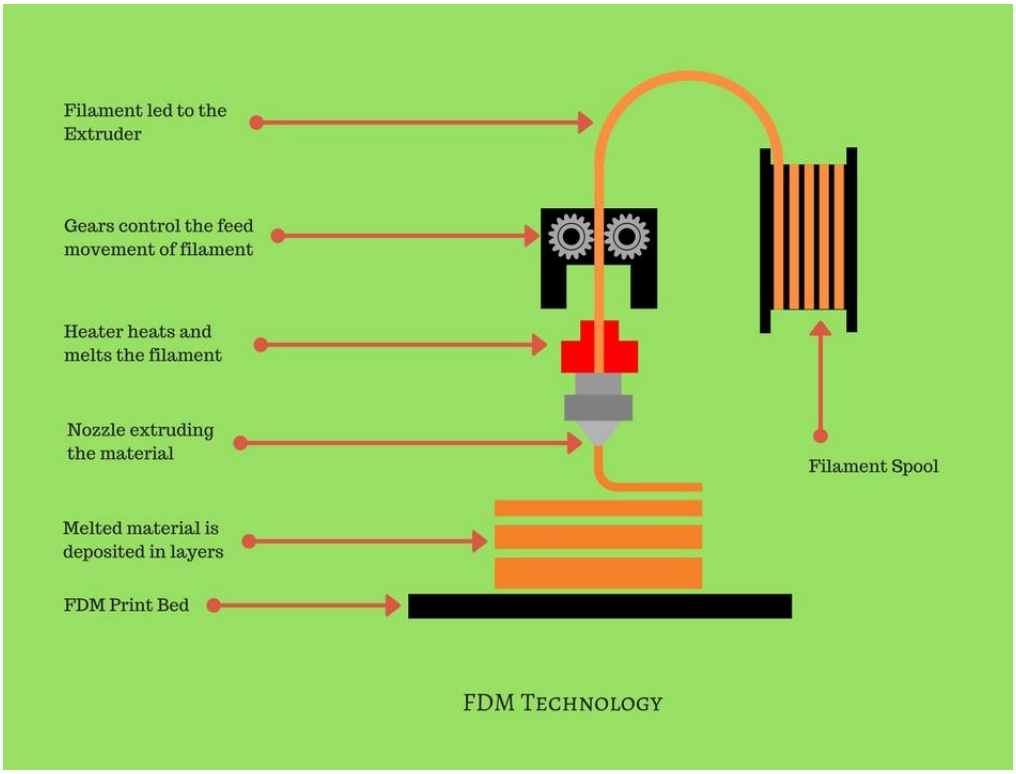

Figure 3. *A schematic of an FDM printer* [17]

In addition to the low-cost machines and a simple process to use the technology, FDM is an economical method to produce prototypes and functional parts within a short period of time. Besides, the supply of the thermoplastic materials is widely available, facilitating the application of prototyping and industrial usages. On the contrary, the technology has a few drawbacks that reduces its efficiency. When comparing the dimensional accuracy and resolution among the 3D printing technologies, FDM possess the least. Furthermore, the visible layer lines and the anisotropic characteristic of an FDM model require the part to be post processed in order to obtain a flat, smooth surface and lessen the inconsistent behaviour. [18]

2.1.2 Printer Parameters

Users can obtain a desired-qualities part by modifying several printer parameters such as build orientation, layer height, infill, printing speed, or the nozzle and build platform temperature. Different settings can have different impacts on the final result, so the operators should consider which options are more suitable for their products. For instance, the smaller the layer height is, the smoother and the more accurate the printed object becomes. This suits the parts whose shape are complex and curved or those parts that require a smooth finish. However, a higher layer height reduces the total production time and it is also more cost-effective. The general FDM layer height ranges between 0.05 mm to 0.4 mm, in which the value of 0.2 mm is commonly applied.

The next important setting that needs to take into account is to generalize a support frame. For some overhang parts, it is impossible to extrude material on thin air. The support structure, therefore, can prevent it by adding more material beneath the main extension features. Nevertheless, it is quite difficult to manually remove support from a small-sized part as the object can be broken. In addition, the removing of support leaves a mark or rough surface so post-treatments may be required. Another more aesthetic way that is applied in industry is using the dual extrusion printer printing the support with a material capable of dissolving in liquid. This method can save the surface from damaging, but it is expensive and only applicable for industrial FDM printers [18]. Hence, it is advisable that the design of a model is optimized so unnecessary support can be avoided.

Printing a fully solid model can result in high production cost with increasing printed filaments and longer printing time. Depending on the properties and application of the final part, operators will employ a proper amount of material printed in the interior structure by adjusting the infill percentage. Infill refers to the inner constitution of the printed part, ranging from 0 % to 100 % [52]. It plays an important role in determining the strength of the whole feature. Higher infill means the part is denser or more solid, allowing the part to possess a better mechanical strength. Infill patterns are also available in various shapes, among of which includes honeycomb, rectangular, triangular or wiggle. [20]

2.1.3 Printing Materials

The choices of material vary for different additive manufacturing processes. They are available in various states such as solid, liquid, and powder. Majority of commercial printing materials are polymers (thermoplastics, thermosets, elastomers), metals, ceramics and composites. A particular process may require a certain type of feedstock to function properly. The material is chosen based on its intrinsic properties as they would have an impact on the performance of the products in a specified application.

In general, both vat polymerization and material jetting utilize photosensitive thermosets (acrylics, acrylates, epoxies) for the printing process. Amorphous and semi-crystalline thermoplastics dominate the materials used in material extrusion. Most of the feedstock of powder bed fusion are semi-crystalline polymers (polyamide-nylon, polyurethane, polyester, polyetheretherkeytone), with a few exceptions of amorphous polymers like polystyrene or polypropylene. In addition to plastics, pure metal (gold, silver) and metallic alloys (Co-Cr alloys, nickel alloys) can be used for this process as well. Binder jetting and directed energy deposition techniques use a wide range of metal and alloys powder such as stainless steel, titanium, aluminium alloys, etc. Sheet lamination can function well with any feedstock in the sheet and powder form (paper, metal powder). [8]

Together with the continuous development of the new types of additive manufacturing processes and printers, scientists and engineers have ceaselessly studied and introduced the industry to the new printing materials. They aim to create a flawless printability feedstock, which solves all the challenges remaining in the current 3D printing materials. Li, N et al. [21] discussed 12 types of new materials from the results of several researches. The scrutinized materials ranges from steel, alloys, superalloys, intermetallic compounds to biomaterials and high entropy alloys.

2.1.3.1 Printing filaments for FDM technique

Material extrusion process, especially in FDM, favours the use of amorphous thermoplastic filaments, with ABS [Acrylonitrile Butadiene Styrene] and PLA [Polylactic Acid] are the two most well-known materials used in this technology. Moreover, the material's

popularity is attributed to their high chemical resistance, abrasion and excellent mechanical properties [9]. The strength can be improved by mixing the thermoplastic with additives or fibres (carbon, glass) as well.

FDM printers use a broad range of filaments from common plastics like ABS, PLA, high impact polystyrene (HIPS) to engineering plastics like nylon, polycarbonate (PC), thermoplastic polyurethane (TPU), acrylonitrile styrene acrylate (ASA), polyvinyl alcohol (PVA), PETG and high performance polymers such as PEEK, polyetherimide (PEI), ULTEM [23]. For the same type of filament, the material properties can differ per manufacturer. Therefore, it is recommended that the users follow the range of temperature for the nozzle and printing bed advised by the producer.

In the aerospace or packaging industry, materials like PEEK, ULTEM, PEI are widely used to produce high-performance application parts due to their high strength, durability, and impact strength. But for a desktop 3D printing filaments, PLA and ABS are the most favourable choices because the materials are low in prices and available in a variety of colours. Besides, ABS can be utilized in many applications that require high strength, temperature resistance, and ductility. [23] Dual extrusion 3D printer is extremely common in industrial applications. A few examples are HIPS which can be dissolved in Limonene or PVA, a water-soluble substance [23].

2.1.3.2 PLA

Polylactic Acid (PLA) is a sugar-based biodegradable and environment-friendly polymer. It is derived from any sugar plants available in the area like corn starch, tapioca, or sugar canes. Its natural properties induce the materials to degrade easily in three to six months [24]. Furthermore, due to the compatibility between PLA and the human body, the plastic is widely applied in tissue engineering, drug delivery systems and bone structures fixing [25]. It is simpler to print with PLA filament than others since the material has a fairly low melting temperature, between 180 and 220℃ [26]. PLA provides a smooth appearance and is a perfect choice for products aiming for the aesthetic rather than functionality. As a result, PLA products tend to be used in rapid prototyping, or other applications that do not require high mechanical properties such as figures, low-wear toys, containers [24]. Another advantage when printing with PLA is warping resistance which is accounted for

the low thermal expansion coefficient [2]. Unlike ABS emitting toxic fumes like styrene, PLA is safe and pose no harmful threat to human health if proper ventilation is installed.

On the other hand, PLA has disadvantages in many aspects as well. First of all, this material is not an option for high heat-resistant products as it quickly melts when heated. PLA also tends to be more brittle and less flexible than other polymers such as ABS or Nylon [24]. Due to its sensitivity to heat, a PLA 3D printed item is not recommended to be put in the dishwasher. The water in the machine is so hot that the part can deform in the form of crack and warping. [22] Additionally, although PLA is made from natural ingredients, its properties can alter after being processed with the addition of both organic and non-organic substances, making it no longer safe for food applications. Water absorption is an extra factor needed to take into consideration when storing the filaments. The material rolls must be kept in tight boxes in order for the filaments to avoid absorbing moisture in the air, which has significant impacts on the prints' outcomes. The damaged filaments could become more and more brittle, and the diameter gets enlarged [24].

The production of PLA filaments starts from blending the transparent, raw granulated plastic with additives and/or pigments. Then, the blend is heated around $60 - 80℃$ before being put into the extruder. The ingredients melt at a certain temperature and get extruded into a filament-form. The filament later is submerged in the warm water first and then in the cold-water tank, when it is ready to be wounded on a roller. [24] The uniformity of the filament's diameter must be ensured, otherwise, it can affect the quality of the final parts [25].

When operating the FDM 3D printer, the nozzle and the build platform temperature are set based on the technical data sheet provided by manufacturer. However, a glue stick or tape is adequate for the extruded plastic to adhere well on the platform. For the filament, it is available in multiple colours and the selections of PLA composites are diverse. Various PLA filament blends can be seen on the market such as PLA mixed with wood, metal powder, carbon fibre, polyester, steel, etc. By adding light sensitive particles, fluorescent pigments, graphene or other polymers, manufacturers can obtain a filament with the capability of changing colour, possessing fluorescent colours, being highly conductive and having increased mechanical strength, respectively [24].

Figure 4. *Spools of PLA filaments* [26]

2.2 Tensile Properties

2.2.1 Tensile Stress – Tensile Strength

A tensile test is done for the purpose of measuring the material's mechanical properties such as ultimate tensile strength, yielding stress, elastic modulus or failure strain, etc. This test is performed by gripping one end of the sample having a rectangular or cylindrical shape with required gauge length L_0 and cross-sectional area A_0 and applying an axial load P on the sample. [27]

The engineering stress is interpreted as the internal force acting on the initial cross-sectional area when subjected to external loadings. When it is subjected to the maximum force, before the fracture of the material, σ is referred to as ultimate tensile stress (UTS), or tensile strength σ_{UTS}. [27]

$$\sigma = \frac{P}{A_0} \tag{1}$$

Where σ: tensile stress [MPa]

P: the external force acting on the plan perpendicular to the longitudinal axis [N]

A_0: cross-sectional area of the reduced section [m^2]

2.2.2 Tensile Strain

Tensile strain or normal strain is the deformation of the materials resulted from the applied stress. In a tensile test, this deformation is produced under forces that are perpendicular to the cross-sectional area of the specimen. It is a unitless parameter and it is equal to the ratio of the change in dimension of the sample to the original length. [28]

$$\varepsilon = \frac{L - L_0}{L_0} \tag{2}$$

Where ε: tensile strain

L_0: original dimension of the material

$L - L_0$: the change in sample's length

2.2.3 Young's Modulus

Young's modulus, named after Thomas Young, represents an elastic material's stiffness. It is also known as tensile modulus, elastic modulus or modulus of elasticity and is equal to the ratio of stress to strain in the elastic region. The elastic behaviour is a straight line in the stress-strain diagram that exhibited before the stress reaches its proportional limit. Higher modulus materials are stronger since they do not stretch much in the tensile test. On the contrary, materials like rubber stretch a lot when being pulled, hence, it possesses a low elastic modulus. ASTM D638 or ISO-527 are the standard tests measuring the tensile properties of plastic materials. [29, 30, 31]

$$\sigma = E\varepsilon \tag{3}$$

Where E: modulus of elasticity [MPa, GPa]

σ: nominal stress [MPa]

ε: nominal strain

2.2.4 Mohr's Circle

Plan stress is a state at a point of the material where it is subjected to two normal stresses and one shear stress, figure 5. The normal stresses σ_x, σ_y and shear stress τ_{xy} are positive when they act in the same direction with the x-y coordinate axes. When these three stresses orient by the angle θ, theirs values are determined by equation (4), (5) and (6). Besides, the anticlockwise orientation of the point defines the positive of the angle θ. [28]

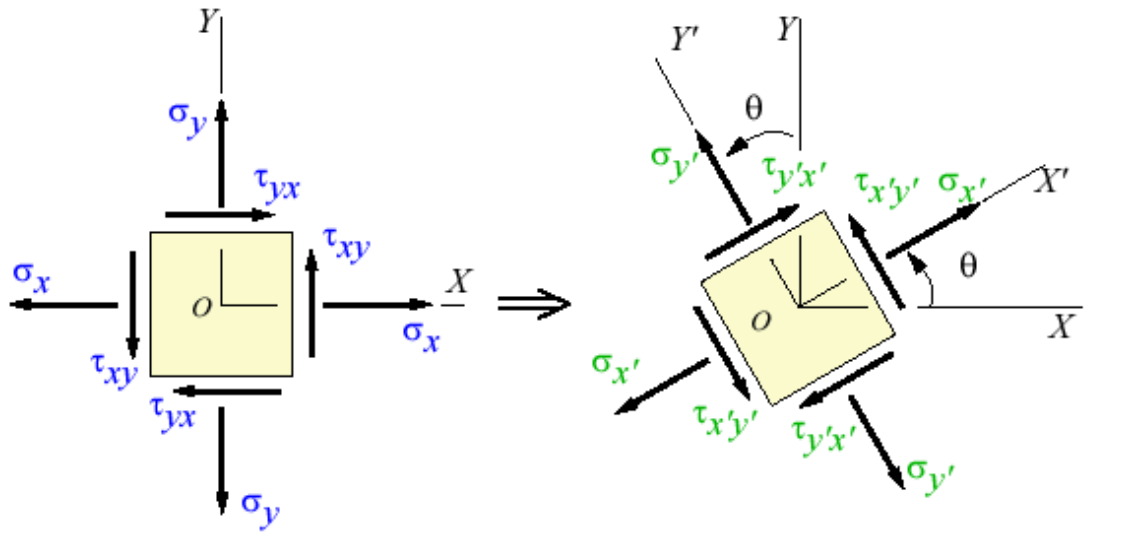

Figure 5. *In-plane stress components of an element* [32]

$$\sigma_x' = \frac{\sigma_x + \sigma_y}{2} + \frac{\sigma_x - \sigma_y}{2} cos\ 2\theta + \tau_{xy}\ sin\ 2\theta \tag{4}$$

$$\sigma_y' = \frac{\sigma_x + \sigma_y}{2} - \frac{\sigma_x - \sigma_y}{2} cos\ 2\theta - \tau_{xy}\ sin\ 2\theta \tag{5}$$

$$\tau_{x'y'} = -\frac{\sigma_x - \sigma_y}{2} sin\ 2\theta + \tau_{xy}\ cos\ 2\theta \tag{6}$$

In 1882, Otto Mohr established a tool, known as Mohr's circle, showing the relationships between normal stresses and shear stress. For the given stress components, stresses at any point lying on the Mohr's circle can be measured, especially the principal stresses σ_1, σ_2 (maximum and minimum normal stress) and maximum shear stress τ_{max}. [28]

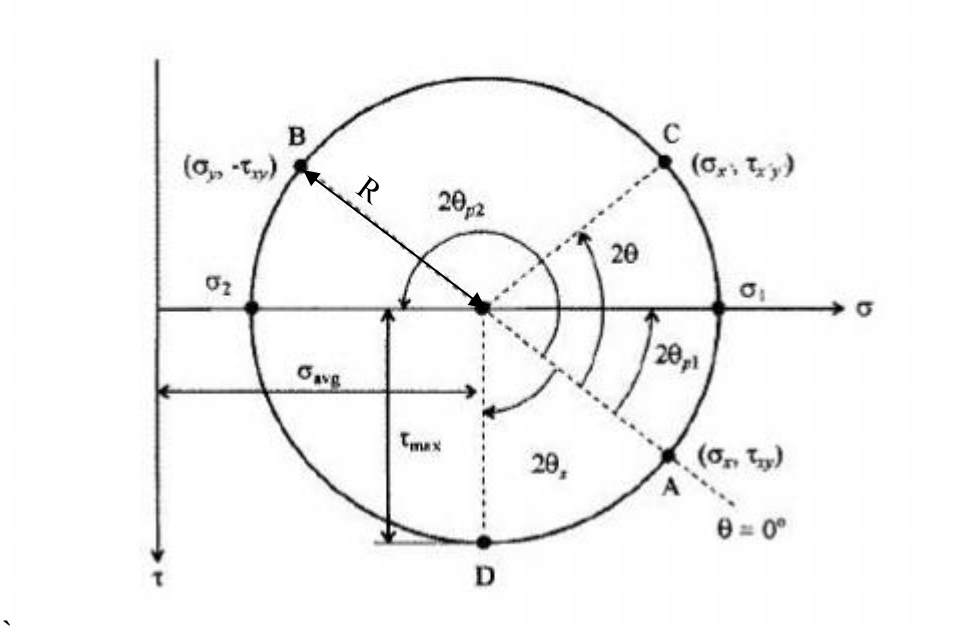

Figure 6. *Mohr's Circle* [33]

As shown in figure 6, point A and B indicate the element's state of stress. The radius *R* of the circle and the average normal stress is calculated using equation (7) and (8), respectively. The values of the principal stresses as well as the maximum shear stress and their corresponding plane orientation from the initial point can be obtained from equation (9) to (12).

$$R = \sqrt{\left(\frac{\sigma_x - \sigma_y}{2}\right)^2 + \tau_{xy}^2} \tag{7}$$

$$\sigma_{avg} = \frac{\sigma_x + \sigma_y}{2} \tag{8}$$

$$\sigma_{1,2} = \frac{\sigma_x + \sigma_y}{2} \pm \sqrt{\left(\frac{\sigma_x - \sigma_y}{2}\right)^2 + \tau_{xy}^2} \tag{9}$$

$$tan\, 2\theta_p = \frac{\tau_{xy}}{\frac{\sigma_x - \sigma_y}{2}} \tag{10}$$

$$\tau_{max} = \sqrt{\left(\frac{\sigma_x - \sigma_y}{2}\right)^2 + \tau_{xy}^2} \tag{11}$$

$$tan\, 2\theta_s = \frac{-\frac{\sigma_x - \sigma_y}{2}}{\tau_{xy}} \tag{12}$$

2.2.5 Stress Concentrations

When an object abruptly changes in geometry caused by sharp corners, cracks or holes (Figure 7), localised stress is accumulated in the cross-section area where the changes are located, which is called stress concentration or stress risers [28]. The stress increases above the nominal or average normal stress, causing the body to fail at the locations where the stress concentration is higher. The stress concentration factor, K_t, is defined by dividing the peak stress to the nominal stress. [53]

$$K = \frac{\sigma_{max}}{\sigma_{avg}} \tag{13}$$

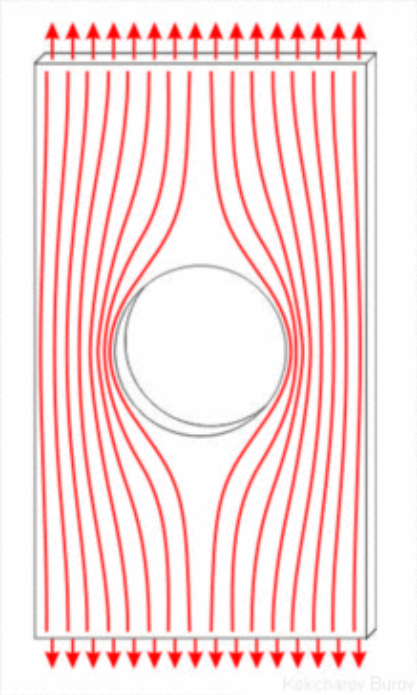

Figure 7. *Stress distribution over the body* [53]

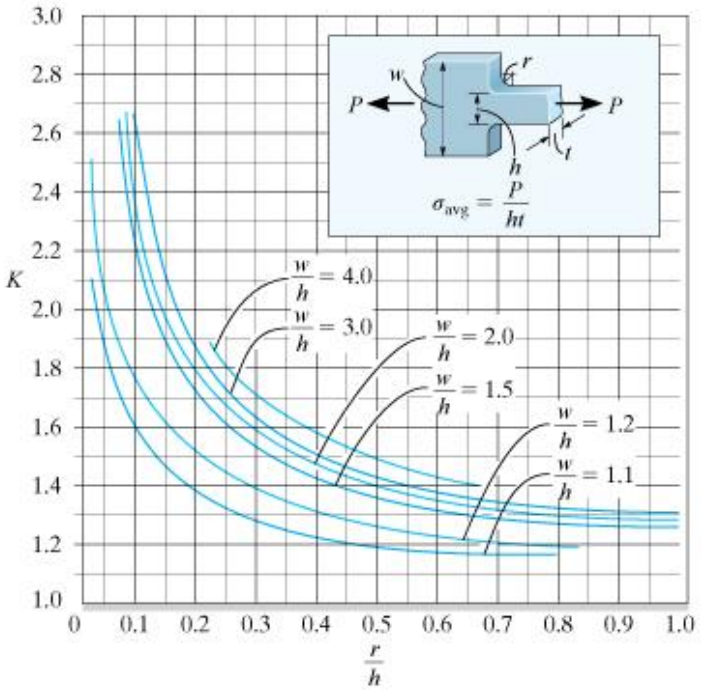

Figure 8. *Stress concentration factor chart* [28]

2.3 Finite Element Analysis (FEA)

The term finite element analysis is originated from the Finite Element Method (FEM), the discretisation of mathematical models into multiple elements and the solving of the discretised equations. Partial differential equations (PDEs) are space and time-dependent descriptions of the laws of physics in the mathematical language. It is founded on the laws for the balance of forces and the relation with stress and strain for structural mechanics. In order to describe the laws, various PDEs with boundary and initial conditions (loads and constraints) can be generated from a model. The boundary conditions provide additional conditions for the solution of a function on the border of the defined area. One model can consist of numerous boundary conditions. The initial condition is the beginning state of a system in a time-variable event. [54]

FEA software has been adopted in companies and institutions for the purpose of predicting the performance of a computational model in reality. It involves using a computer-aided design (CAD) part and the provision of the information of the applied force and

material properties. The level of accuracy can be improved by a process called mesh refinement. The mesh divides the model into smaller and smaller finite elements, each of which is governed by a set of equations. When the mesh is refined, the simulated solution reaches the true answer. An FEA model, when generated, can reduce the prototypes needed to produce and optimise the design of a device or process. [55]

2.4 Microscopy Methods – Optical Microscopy

The emergence of new materials with their new characterizations in the past few years has intrigued the scientists to look into the word of materials in atomic and molecular levels. Various microscopy, scanning or imaging analysis techniques were invented and improved for the purpose of obtaining the full data about the material's structure, properties, and the way it was processed. These methods can be applied in the qualitative analysis as well as quantitative analysis [34].

The analytical techniques vary depending on the result requirements. In general, the currently common technologies used to determine polymer properties are wet chemistry; X-ray scattering; thermal, spectroscopic, chromatographic and microscopy methods. They characterize the material physics by the dispersion of light, x-rays, neutrons or by the image fabrication through the microscopes. The first techniques examine the specimens in a large area while the latter focus on a specific location. In addition to the different mechanisms, each technology includes several subcategories which test the materials in diverse areas, depths, structures. For instance, spectroscopic methods, generally used to identify certain chemical functional groups and physical characterizations, consist of a wide range of techniques: Ultraviolet-visible (UV-Vis) spectroscopy; mass spectroscopy (MS); infrared (IR) and near-infrared (NIR) spectroscopy; Raman; nuclear magnetic resonance (NMR). UV-Vis spectroscopy and MS mainly scrutiny the broken pieces from the main material. IR instruments have high sensitivity, which is suitable for applications requiring precision. Raman is utilized for small particles, and NMR provides information on both the material and the sample surrounding. [35]

Similar to the spectroscopic methods, microscopy includes multiple analytical techniques that investigate the sample's morphology and fine structure using a microscope. Morphology is connected to the study of the form and size of features whose dimensions are under the specimen size but above the atomic scale. These features can be additives, fillers, fibres, or macrostructure units. This study is based on the observation and understanding of images formed by the microscopes. In order to fully define the structure-property relationship of a material, one must select a proper analytical technique, understand its advantages and disadvantages, and develop the preparation solutions for the sample investigated. [35]

A few prominent microscopies are optical microscopy (OM); scanning electron microscopy (SEM); transmission electron microscopy (TEM); scanning probe microscopy; and x-ray scattering, in which SEM is the most well-known method. They work upon different principles and analyse several features of the polymer materials in peculiar sizes ranging from nanometres to millimetres. These techniques are also available in numerous resolutions, contrasts, magnifications, and depths of field. [35]

Amongst the microscopy methods, optical microscopy (OM) or light microscopy is one of the oldest technologies and it uses visible light to inspect the sample. There are two types of optical microscopes: simple microscopes and compound microscopes. The first instruments have only one lens and work like a magnifying glass. The second type of microscopes is installed with more than one lens, increasing its magnification, resolution and therefore, they are able to look into smaller details of the sample. Another common device is digital microscope, which is directly linked with a high-quality digital camera and the images produced are shown on a computer for further analysis. [35]

An optical microscope, as shown in figure 5, has seven basic components: ocular lenses (eyepieces); tube; objective lenses; stage; condenser; focus; and light source. More than one objective lenses with different magnifications are held by the objective turret so the operators can change between these lenses. Moreover, the condenser acts as a light collector, ensuring the illumination sources are focused on the specimen. The microscope's magnification typically ranges from 2 to 2000×. This entire magnification figure is obtained by multiplying the magnification of the ocular and objective lenses. [35]

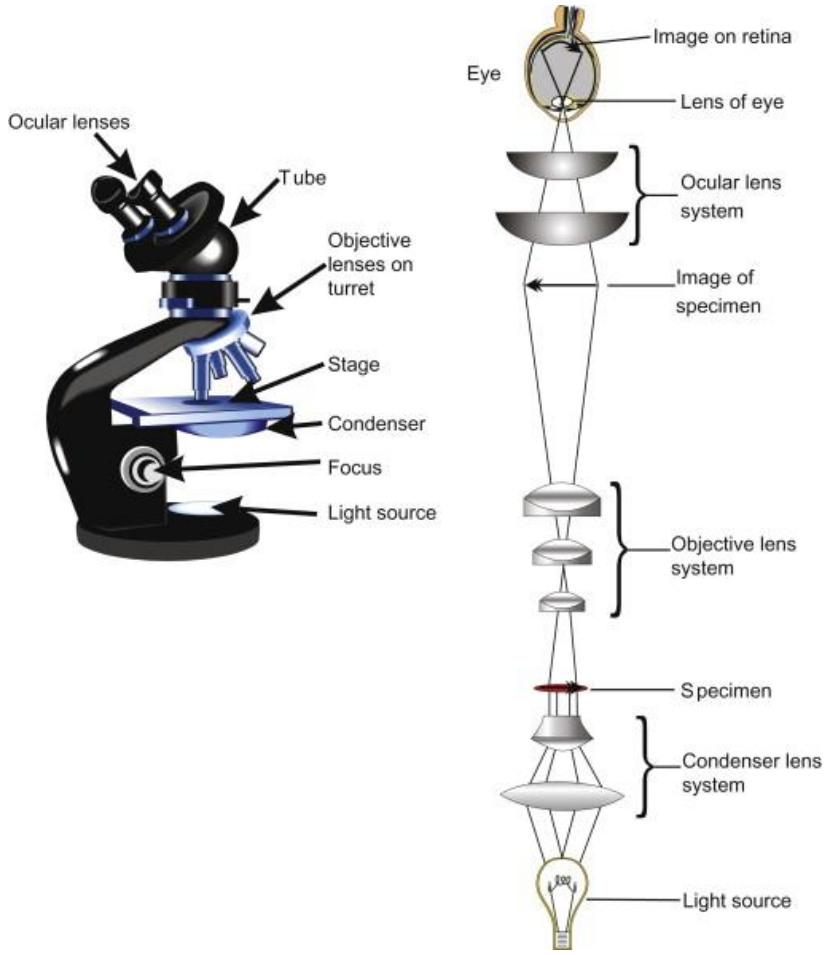

Figure 9. *Optical microscope* [36]

The device has two basic light modes: transmission and reflection mode. Regarding the imaging modes, the technique is divided into four categories: bright field, dark field, phase contrast and differential interference contrast (DIC) microscopy. In the bright field, the specimen tends to be darker than the background through the eyepieces as it absorbs some light from the light source. On the contrary, the specimen appears brighter in dark field microscopy, making it suitable for transparent parts. Phase contrast is a type of microscopy improving the contrast of the sample by the difference in the interaction between the components' densities and the illumination. Finally, the DIC instrument is sensitive to the change in depth and reflective index, which allows the determination of the specimen thickness. [37] Besides, the technique prefers using reflective light due to its simple apparatus [35].

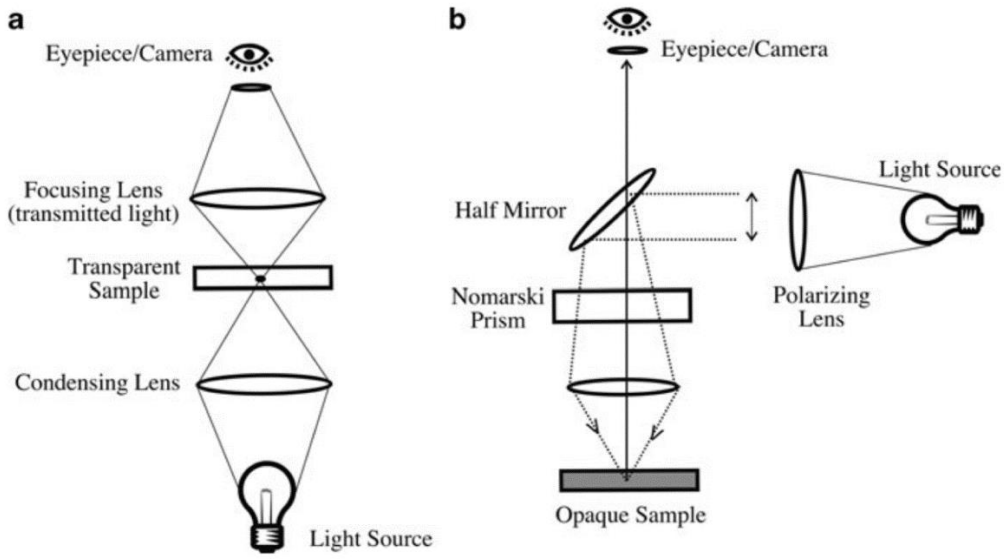

***Figure 10**. a) Transmitted light microscope; b) Reflective light microscope* [38]

When operating an optical microscope, users must first select the appropriate magnification and adjust the contrast. Then, adjusting the focus knob to move the stage up and down or left and right in order to find the focal plane. Lastly, when we are able to identify the specific feature, pictures are taken by a camera before the final step, image interpretation. [39]

2.5 Product Design

The unceasing progress in prototyping technology, the availability of the computer-aided design software and finite element analysis tools have captivated more designers to the world of 3D printing, where you can create products in shorter time and with higher accuracy. However, a successful design is not defined based on the designer's skills and ideas, there are several prerequisites about the designing process needed to be contemplated in order to design functional models that meet all the requirements.

The design process of a new product line or invention originated from companies may include multiple teams from different sectors working in the same project. The whole process in general starts from the product plan, which is regarding the introduction of the new concept, to the design part then manufacturing, logistic, marketing and sales [40]. The plan must specify the overall estimating cost for the manufacturing and distribution

process, along with the information of the materials and equipment suppliers. The marketing team can also use this plan to survey the customers' opinion about the new product. In this way, the companies not only focus on targeting their potential clients in the future, but also increase the opportunity to expand the market to other groups of customers.

For individuals, the process can be simplified into three steps: determining the product requirements, deciding printing material(s) and optimizing function and appearance [40]. One of the essential factors in the first step is to identify the function of the model because the way it is used will define further conditions such as material properties, temperature requirements, environmental/chemical exposures, life expectancy, aesthetics, etc.

Firstly, the total operating range of temperature that the part will experience needs to be evaluated. A few properties like tensile, impact strength or coefficient of expansion change according to the temperature [40]. For instance, the modulus decreases with the rise in temperature as the increase in the molecular vibrations causes the part to deform greater. As for the impact strength, it also increases at elevated temperature since the material becomes less rigid and is able to absorb more energy before fracture. Moreover, the stress-strain curve for plastics only shows the material's Young modulus or tensile strength at a particular temperature and loading rate, without anticipating these properties at different conditions.

Next, checking the requirements for the part's mechanical properties (tensile strength, impact strength, rigidity, hardness) and whether the part will undergo any static, cyclical or vibrational loadings. If the part is subjected to static load or creep data, response of the material to the loading, are used in order to predict deformations over a period of time. On the contrary, plastic objects subjected to a certain number of cyclical loads fail within the material in the form of microscopic cracks due to the accumulated damage. Therefore, it is advisable not to design sharp corners, changing thickness and holes as well as avoiding designing the weld lines in the stressed location for cyclical loading parts. [40] The thorough consideration of the above-mentioned requirements is the key for the designer to select a proper material for the application.

The choices for the feedstock are varied, but most of the common filaments for FDM printers are thermoplastics such as PLA, ABS, Nylon, PE, etc. Fully understanding the

extent of the operating temperature makes the process less complicated since the change in material properties at increased temperature differs depending on the plastic used.

Lastly, producing a prototype can optimize and ease the whole process. By doing this, defects in the design are found and necessary corrections can be made easily by fixing the CAD drawing file. For example, the fitting between parts or surface smoothness can be checked before printing the final applications.

3 METHOD

In order to study and explain the effect of printing parameters on the mechanical properties of the 3D printed specimens, the experiment is divided into three stages: designing and 3D printing process; tensile testing; and microscopic examination. This section firstly introduces to the readers the material and the experimental apparatuses supported for the practical work. Then, the procedure about the preparation, equipment settings and the choice of the testing parameters of each stage was clearly explained below. A description of the process of generating and testing a computational model in the COMSOL software is also included in the last part.

3.1 Material – Equipment

3.1.1 PLA

The material used for this work is the $1.75\ mm$ in diameter PLA filament provided by MakerBot. The filament is mentioned to have a glass temperature ranging from 60 to $65℃$, a melting temperature of $150 - 160℃$, and the nozzle temperature is recommended to be set at $215\ ℃$ [41].

Material properties of PLA $(C_3H_4O_2)_n$ are presented in the table below:

Table 1. *Material's properties of PLA* [42]

Density	1.23 -1.25 g/cm^3
Elongation at Break	3.8%
Tensile Strength	57.8 MPa
Tensile Modulus	3.3 GPa
Moisture Absorption	Minor
Surface Quality	Good

3.1.2 MakerBot 3D printer

All the samples were printed with the MakerBot Replicator 5th Generation, which uses the fused deposition modelling printing technology. The printing filament is also manufactured by the same company with a diameter of 1.75 mm. This generation printer is connected to a smart extruder whose diameter is 0.4 mm. The 3D design of the test piece is first converted to a STL file and is saved as a THING file ($.thing$), a file format that stores information about one or multiple 3D models' location, orientation and other printing settings, in the MakerBot Desktop Software. It is then exported to $.makerbot$ file type in order to be interpreted by the printer.

3.2 Sample Preparation

3.2.1 Sample preparation for 3D printing process

The testing sample type 1A was designed on the SolidWorks 2019 software according to the standard of ISO 527-2:2012. The dimensions [mm] of the sample shown in Figure 11 are listed in Table 2.

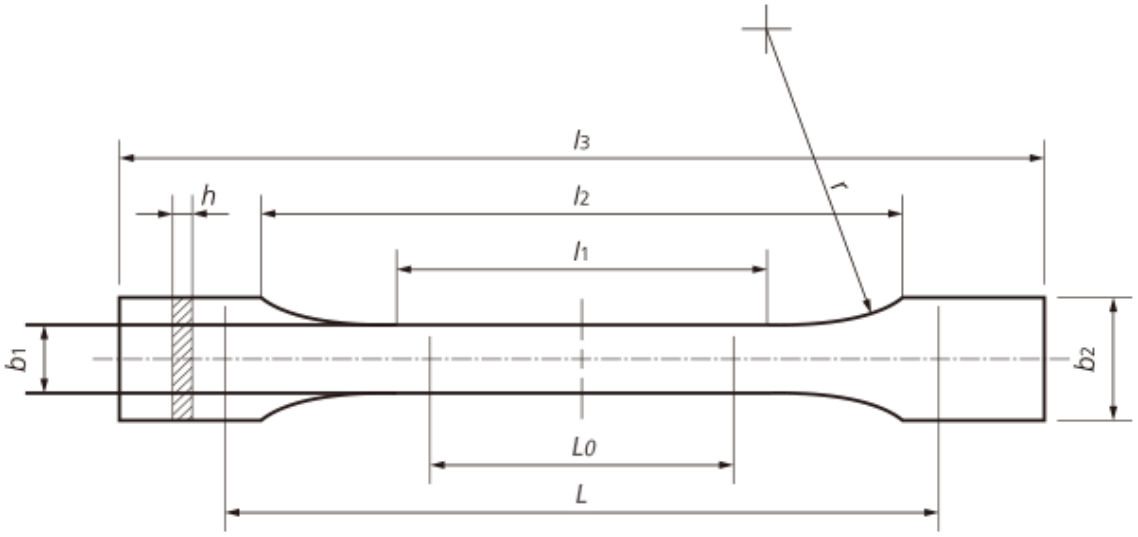

Figure 11. *Test sample sketch* [43]

***Table 2**. Test piece dimensions* [43]

l_3	150 mm
l_1	80 mm
r	20.725
l_2	107 mm
b_2	20 mm
b_1	10 mm
h	4 mm
L_0	50 mm
L	115 $\pm$ 1 mm

As a CAD model has been created, the file was converted to an $.stl$ format to be interpreted by the MakerBot software. The samples will be printed with the parameters that are assumed to directly affect the properties of the models. The work was divided into two parts. The first part included printing and testing the samples printed in three main orientations: XY (flat), XZ (on-edge) and ZX (upright), shown in Figure 12. The toolpaths for particular orientation generated by the software can be observed in Figure 13 and based on the research of Ahn, S.H et al [44], the part whose raster angle (or raster orientation, the direction of the raster pattern relative the applied loading [60]) is perpendicular to the axial (tensile) loads possesses the lowest tensile strength when compared to the other two orientations. This prediction is later confirmed in section 4 by the results of the corresponding tensile tests. Therefore, the following samples are printed only in XY and XZ plane along with other control parameters. These parameters are decided to be infill density (10%, 50%, 95%) and layer height (0.1 mm, 0.2 mm, 0.5 mm). For each type of the specimens, except the selected parameter, the remaining settings are kept default according to the MakerBot software. Therefore, there are 11 types of sample (Table 3) in total in this experiment. For each type of settings, two models will be printed and tested in order to get the average value of the tensile properties.

Table 3. *Printing parameters chosen for each type of sample*

Type	Build Orientation	Layer Height	Infill
1	Flat	0.2 mm	10%
2	On-edge	0.2 mm	10%
3	Upright	0.2 mm	10%
4	Flat	0.1 mm	
5	Flat	0.5 mm	
6	Flat		50%
7	Flat		95%
8	On-edge	0.1 mm	
9	On-edge	0.5 mm	
10	On-edge		50%
11	On-edge		95%

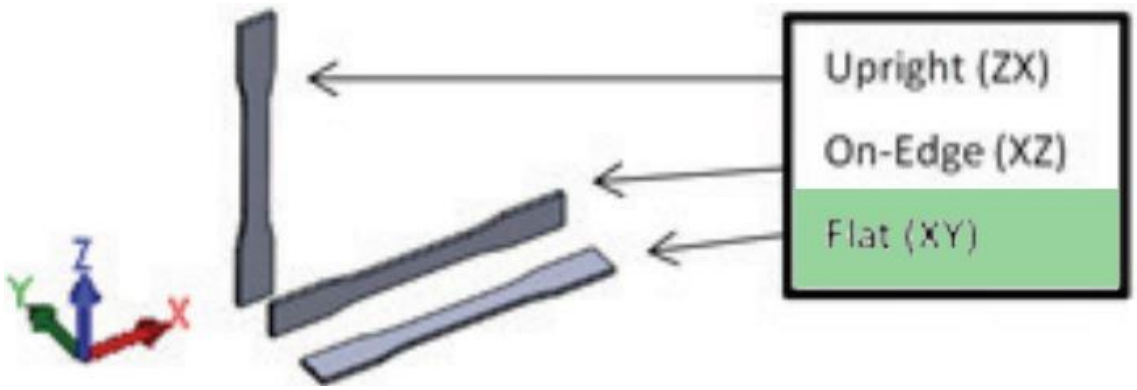

***Figure 12**. Three basic orientations of a print* [45]

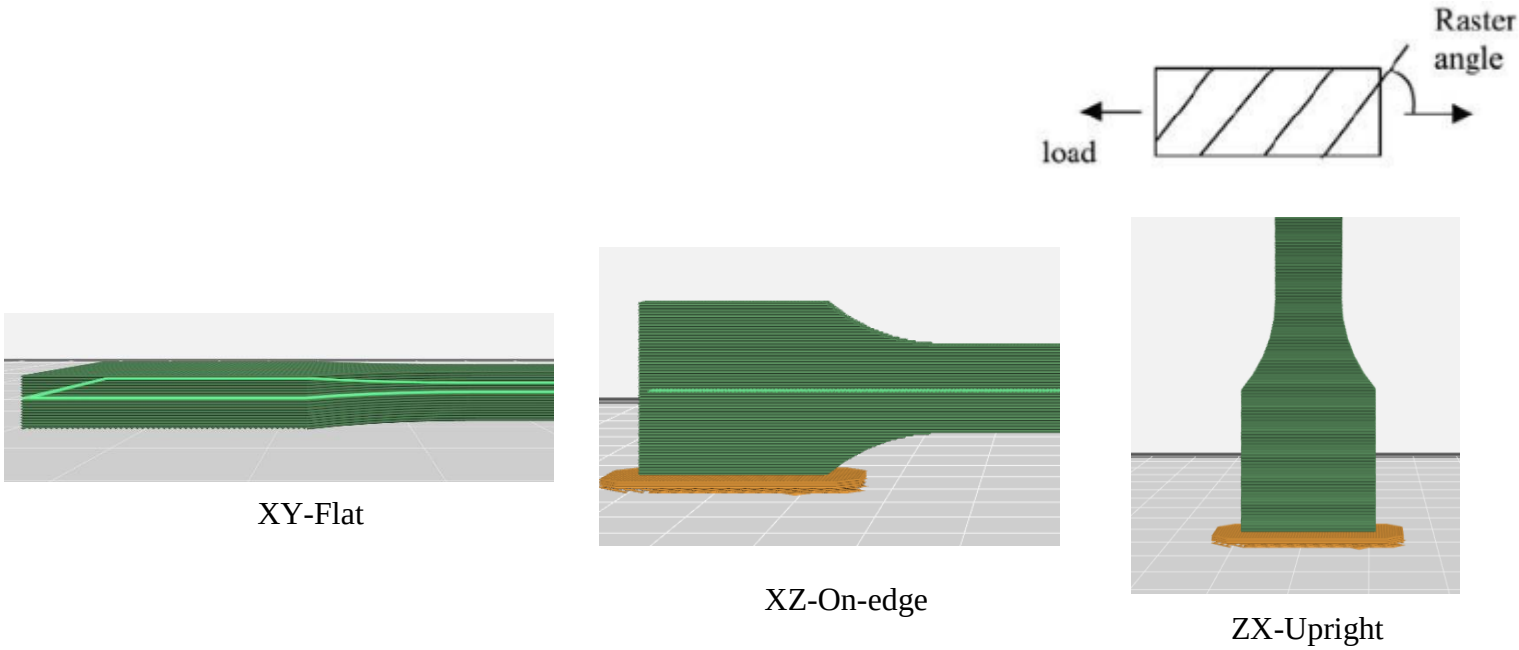

***Figure 13**. Toolpath generated by MakerBot software*

3.2.2 Sample preparation for optical microscopy

In this experiment, the Zeiss Axio Scope A1 light microscope, available at Arcada's chemistry laboratory, was utilized for the purpose of observing the cross-section of the fracture surface. The equipment can be adjusted to reflective, transmitted or polarized light depending on the type of sample used or the user's aim. Five levels of objective magnification are available, including 5x, 10x, 20x, 50x and 100x. [46] A Canon camera is mounted on the top of the microscope and is linked to a nearby computer where the

images of the sample observed are shown. Additionally, the photos taken are retrieved from the computer memory.

In the preparation process, three ways of preparing the tensile-testing 3D printed samples were carried out in order to select the methods that give the desired information from the microscopy study. The first solution was directly observed the tested samples placed on the microscope stage. The following methods aimed to cut the specimens' cross section into small pieces for better observation with a small knife, a scissor and a microtome machine, operated by applying pressurized gas to control the hard steel blaze cutting the samples. Due to the big gap inside the samples, resulting from the low infill chosen from the printing procedure, the surface where the blade went through was not cut straight. The same outcome was obtained for the sample cut with the knife. Therefore, these two techniques were not chosen to produce microscopic-specified samples. Only the first approach was used to study specimens with varying layer thicknesses and orientations.

The last step was to glue the specimens on the microscope slice with an adhesive black tape. These glasses were hold on the stage by two grips. For this study, the reflective light in dark mode and the 5x objective lens were used to observe the samples. The resulting images can be perceived either from the computer screen or the ocular lenses.

3.3 Tensile Testing

The tensile test for printed specimens shown in figure 11 was carried out using the Testometric machine at the Arcada's plastic laboratory. The procedure includes holding the sample tightly between two grips of the tester. A new test definition was created, where the fundamental parameters of the testing sample were inserted: the testing length (gauge length), width and height were set to be 50 mm, 10 mm and 4 mm, respectively. The purpose of the tensile testing is calculating the material's strength, stiffness and the elongation of the specimen to the rupture point. Besides, the Testometric program automatically generates a stress-strain diagram based on testing length (L_0) and the cross-sectional area ($A = b_1 \times h$) provided from the test definition. The test was done at the speed of 5 mm/min and the following parameters (stress, yield stress, maximum tensile strength,

stress at break and strain at break, as well as Young's modulus) were measured by the machine during the procedure.

3.4 COMSOL Modelling

COMSOL Multiphysics is a platform where users can create a model and simulate processes in all engineering fields. Geometries, material properties can be defined to describe a real-world issue and the models are postprocessed to give the accurate results. In this simulation, FEA method is used to find out the principal stress.

- Selecting Model Wizard to create a Stationary study with Solid Mechanics interface in a 3D Space Dimension. The unit for the model is in mm.

- Importing the dog bone sample SolidWorks ($.stl$) file (Figure 14).

- As the material, PLA, for this model was not available in the COMSOL Material Library, a new Blank Material was created. The primary material's properties were inserted, shown in Table 4.

- For Parameter I (Table 5), a force (F) of $1000\ N$ was used in this simulation.

- The bottom surface of the sample was chosen as Fixed Constraint, indicating one end of the part was kept firm. The Boundary Load F in the x direction would be applied on the model's top surface.

- A mesh was built on Finer Element size (Figure 15).

- Finally, the simulation was computed. The results od the study are evaluated by plotting the principal stress and maximum/minimum values.

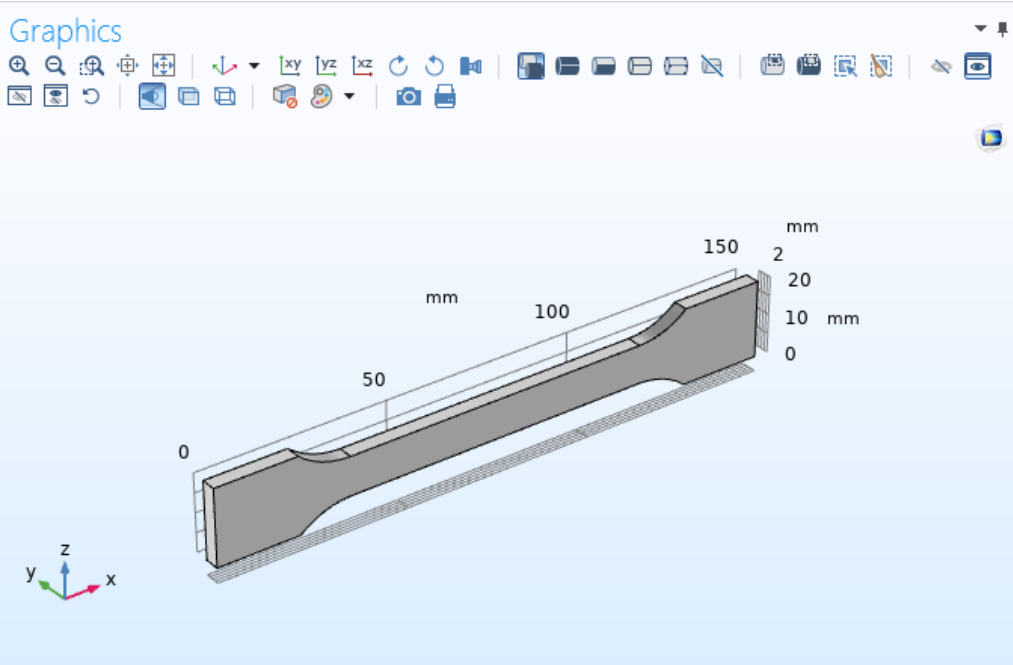

Figure 14*. The imported dog bone in COMSOL*

Table 4*. Basis properties of PLA*

Property	**Variable**	**Value**	**Unit**
Density	rho [ρ]	1250	kg/m^3
Poisson's ratio	nu [ν]	0.33	1
Young's modulus	E	3300000000	Pa

Table 5. *The model's Parameter I*

Name	**Expression**	**Value**	**Description**
F	1000 [N]	1000	Applied force

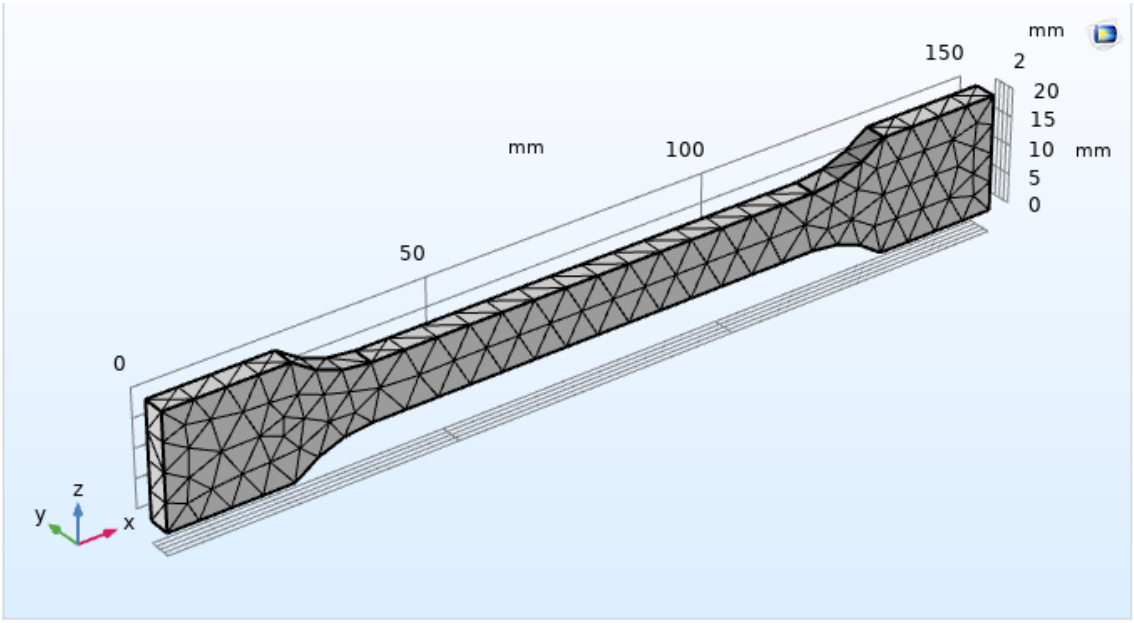

***Figure 15**. Mesh generated by COMSOL*

4 RESULTS

4.1 Mohr's Circle Calculation

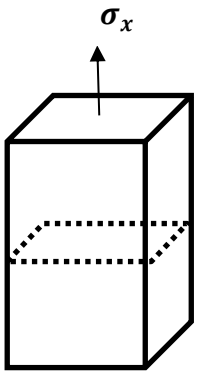

***Figure 16**. Normal stress acting on one end of the specimen*

During the tensile test, the samples were only subjected to the loading at one end, with the state of plane stress shown in Figure 15. The applied force has the value of $1000\ N$, and based on Equation (1), we get:

$$\sigma_x = \frac{P}{A} = \frac{P}{b \times h} = \frac{1000}{10 \times 4} = 25\ MPa$$

As the result, the three known constants are: $\sigma_x = 25\ MPa$; $\sigma_y = 0$; $\tau_{xy} = 0$

`For the construction of the Mohr's Circle, the following parameters are measured based on Equation (8) and (7):

$$\sigma_{avg} = \frac{\sigma_x + \sigma_y}{2} = \frac{25 + 0}{2} = 12.5\ MPa$$

$$R = \sqrt{\left(\frac{\sigma_x - \sigma_y}{2}\right)^2 + \tau_{xy}^2} = \sqrt{\left(\frac{25}{2}\right)^2} = 12.5\ MPa$$

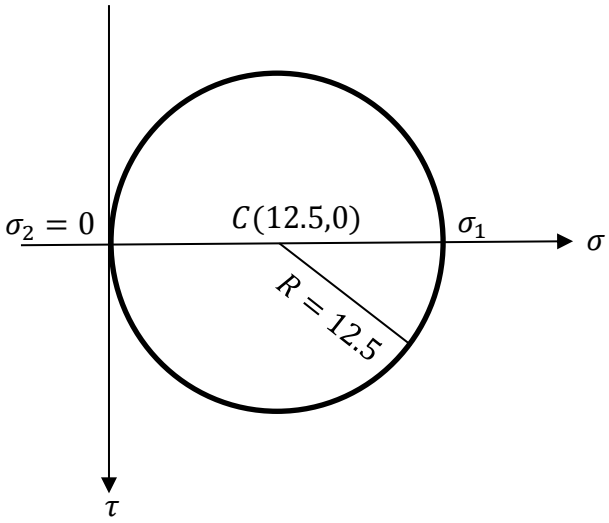

Figure 17. *Mohr's circle construction*

Finally, the maximum normal stress σ_1 is obtained from Equation (9):

$$\sigma_1 = \sigma_x = 25\ MPa$$

4.2 Stress concentration factor

Based on Figure 8, with $\frac{w}{h} = \frac{20\ mm}{10\ mm} = 2$ and $\frac{r}{h} = \frac{5\ mm}{10\ mm} = 0.5$, the value of stress concentration factor K_t is recorded to equal to 1.4. The maximum stress, therefore, is measured using Equation (13):

$$\sigma_{max} = K_t \sigma_{avg} = K_t \frac{P}{bh} = 1.4 \frac{1000}{10 \times 4} = 35\ MPa$$

4.3 COMSOL Simulation

The model generated by COMSOL tool is similar to the one used in the mathematical method, which means the properties of the part are uniform and the same in all directions. Figure 18 presents the principal stress plotted by the software, that shows the result of the stress distribution over the whole body of the model under the load of 1000 N. The maximum principal stress, whose value is 29.41 MPa, located at the radii connecting the narrow and broad parallel-sided portion.

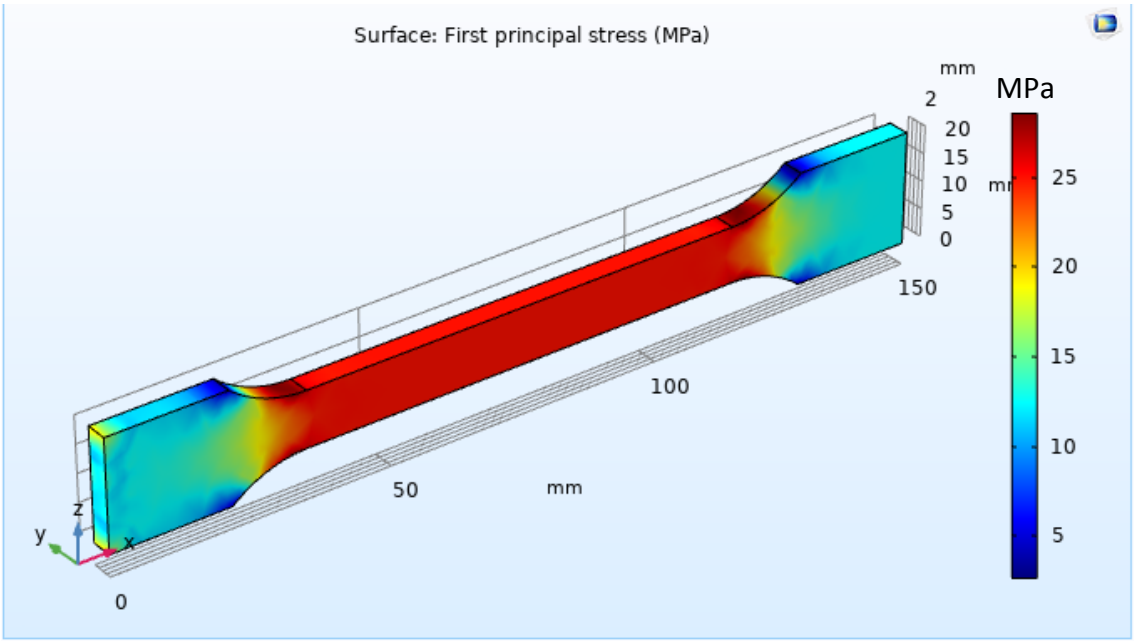

Figure 18. *Principal stress result*

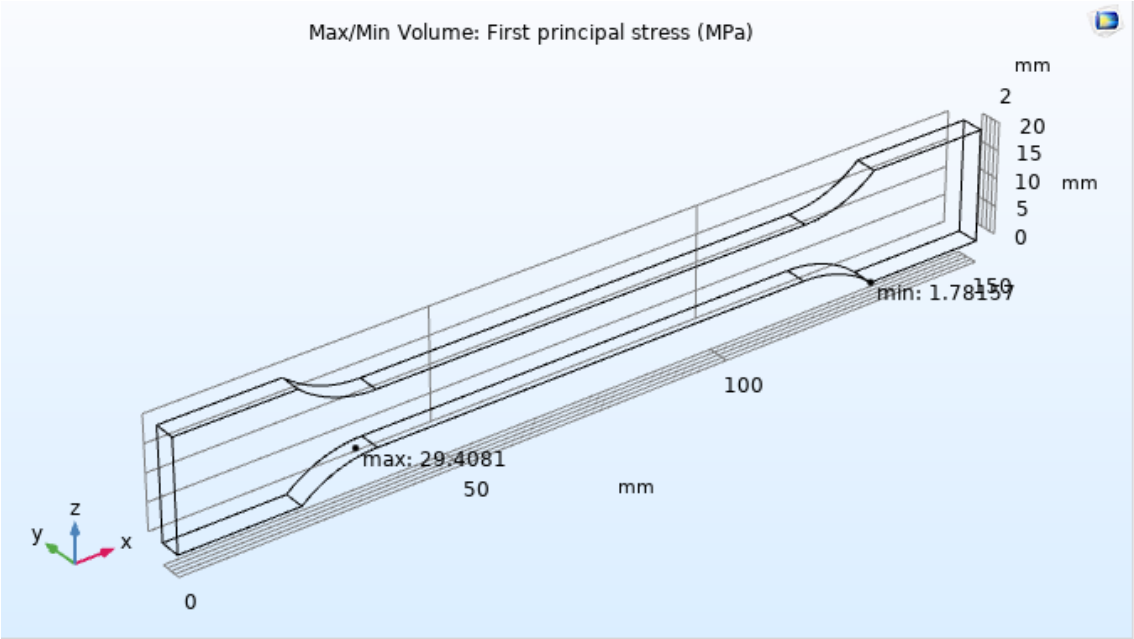

Figure 19. *Maximum and Minimum principal stress result*

4.4 Tensile Testing Results

4.4.1 Build Orientation

The first tensile tests were carried out examining specimens printed in three orientations (XY-flat, XZ-edge, ZX-upright), other setting parameters in which a layer thickness of 0.2 mm and an infill of 10% were kept default. Figure 20 shows the stress-strain diagram of samples in these orientations in the first test and Table 6 presents the average values of tensile properties of two samples printed in the same direction. As the software can create stress-strain curve for only one specimen, the values of tensile stress and strain of each specimens were recalculated and combined together, resulting in the graph below.

Table 6. *Tensile properties of specimens printed in three primary orientations*

Orientation	**E [MPa]**	**UTS [MPa]**	**Stress at break [MPa]**	**Strain at break [%]**
XY-Flat	608.05	22.158	22.071	4.662
XZ-Edge	674.99	22.484	22.17	4.069

ZX-Upright	605.54	18.98	18.98	3.66

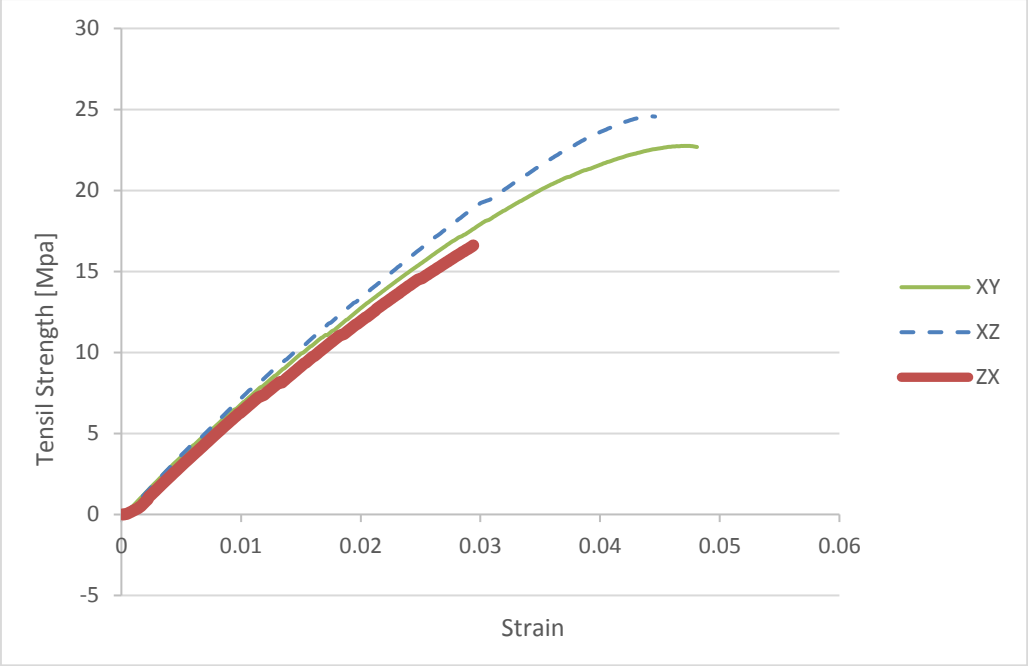

Figure 20. *Stress-strain curves of samples in 3 orientations*

4.4.2 Infill and Layer Height

Similar to the first test, the second tests were conducted for FDM samples in different layer heights and infill. Elastic modulus (E), ultimate tensile strength (UTS), stress and strain at break were determined and illustrated in Table 7. This experiment focused on studying the tensile properties of PLA samples calibrated in several settings, with the main emphasis on the printing orientation. Four charts regarding the maximum tensile stress and elongation at break for two directions but with the same surveying factors were created for further analysis and were presented in Figure 21 and Figure 22.

Table 7. *Tensile properties of specimens printed with different infill and layer thicknesses*

Orientation		**E** $[MPa]$	**UTS** $[MPa]$	**Stress at break** $[MPa]$	**Strain at break [%]**
XY-Flat	**0.1 mm**	636.212	23.91	23.875	4.905
	0.5 mm	727.1	27.787	27.63	5.21
	Infill-50%	632.62	28.93	28.81	5.992
	95%	932.21	41.04	40.833	6.141
	0.2mm/10%	608.046	22.158	22.071	4.662
XZ-Edge	**0.1 mm**	628.807	23.13	22.943	4.389
	0.5 mm	563.816	21.535	20.115	5.083
	50%	749.866	30.183	29.864	4.881
	95%	852.083	39.29	39.166	5.634
	0.2mm/10%	674.994	22.484	22.146	4.069

(a)

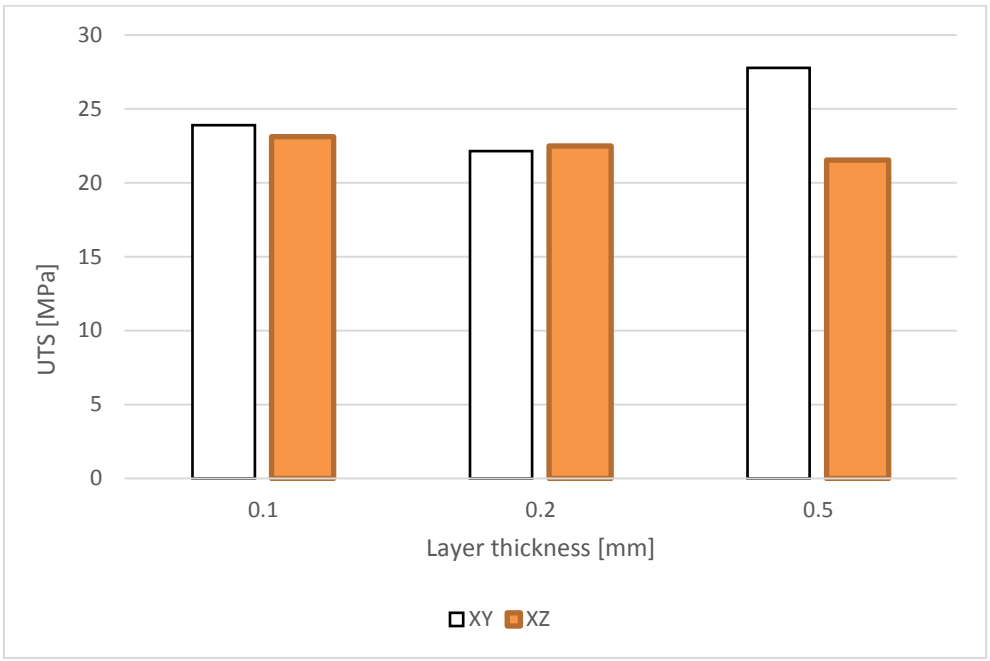

(b)

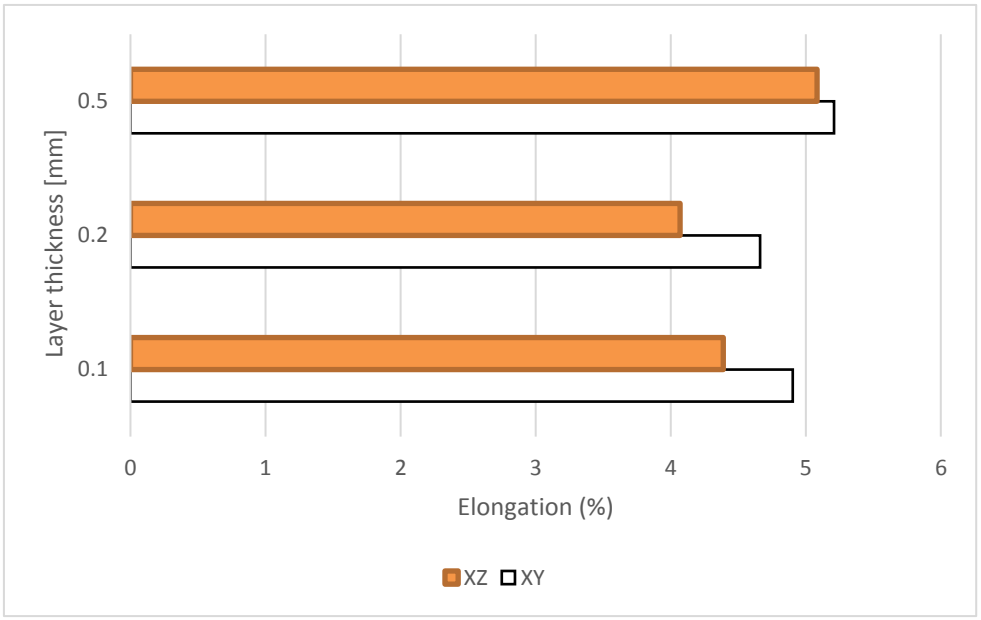

Figure 21. *(a) Strength (b) Strain at break of specimens having the same layer thickness in XY and XZ orientation*

(a)

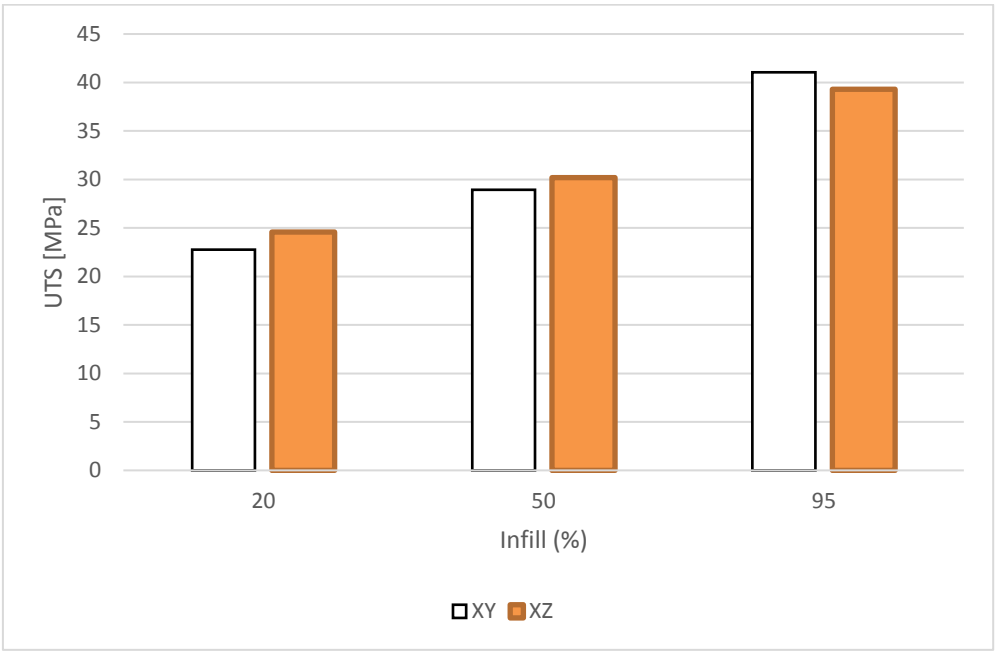

(b)

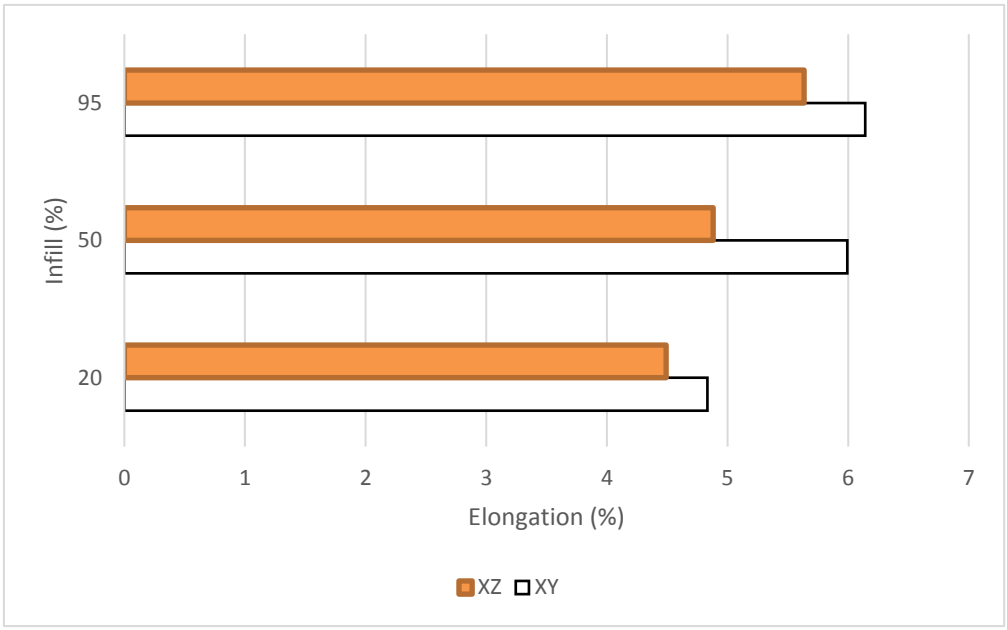

***Figure 22**. (a) Strength (b) Strain at break of specimens having the same infill in XY and XZ orientation*

4.5 Microscopy Results

Figure 23 presents the images of the broken 3D printed dog bones that were held directly on the stage under the microscope reflective light. All the samples, printed in the on-edge orientation in three layer thicknesses: 0.1 mm, 0.2 mm and 0.5 mm, respectively, were observed at the edge of the cross section where it is fractured. Additionally, figure 24

shows the fracture cross section of FDM fabricated part in three primary direction under 5x magnification.

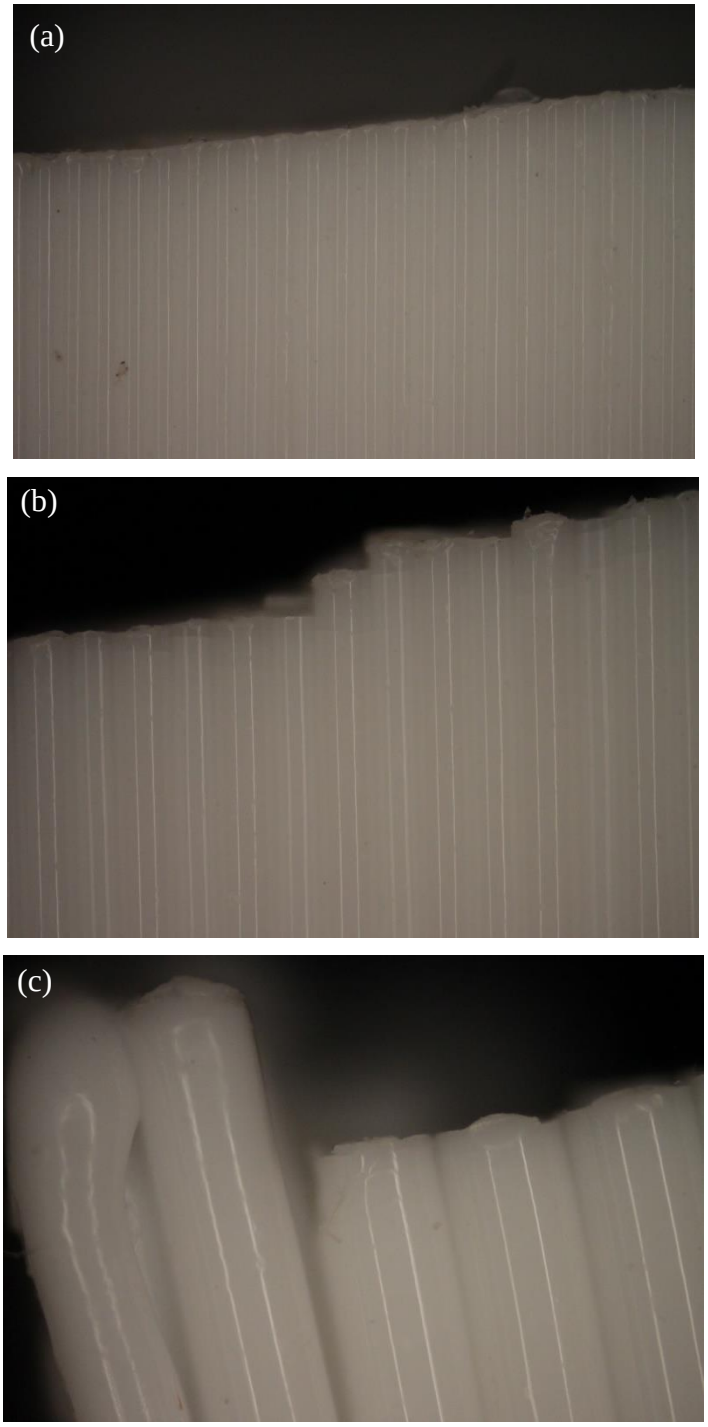

Figure 23. *OM images of the fracture cross section's edges of samples in several layer thicknesses. (a) 0.1 mm, (b) 0.2 mm, (c) 0.5 mm*

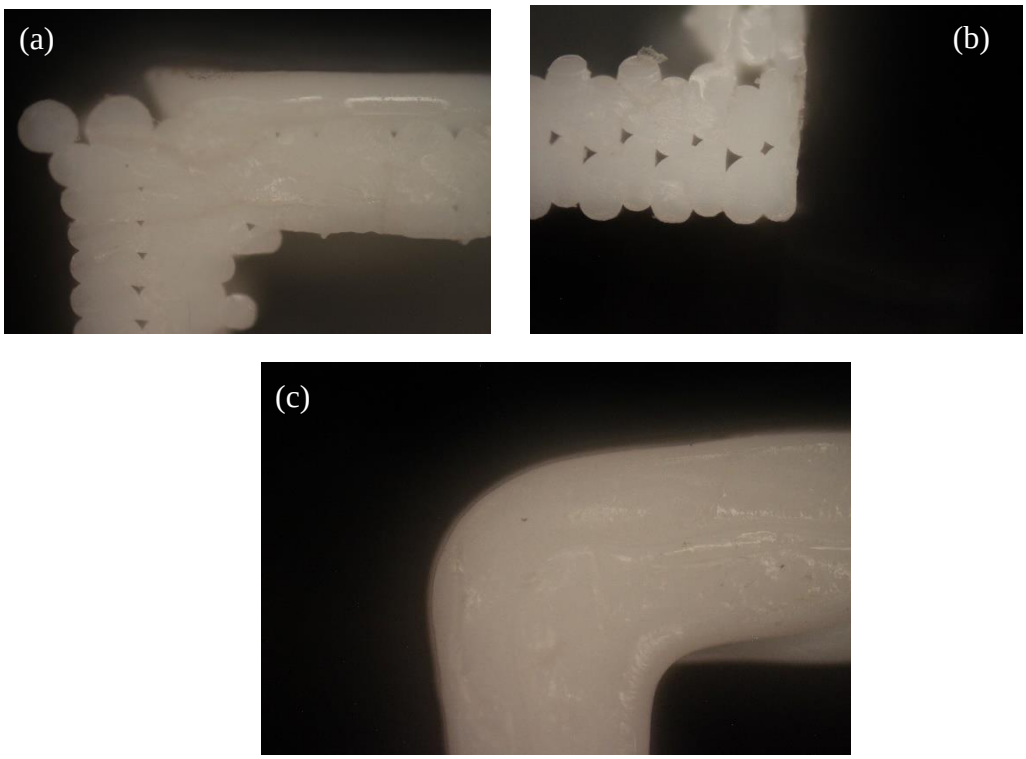

Figure 24. *OM images of fracture cross section of FDM parts in 3 orientations. (a) Flat, (b) On-edge, (c) Upright*

5 DISCUSSION

5.1 Mathematical and Computational Analysis

Both the COMSOL and mathematical methods were set in the same condition (using the same amount of force as well as sample's dimensions) for predicting the principal stress. The results of these three approaches are compared, indicating that the maximum normal stress measured by computational method is 17.64% larger and 16% lower than ones calculated by the Mohr's circle method and by the stress concentration factor, respectively.

The purpose of adopting the analytical and computational method in this work is to estimate the mechanical properties of the corresponding 3D printed part. An important note is that the model used for the static analysis is solid, while the experimental models have porosities in the inner structure. The principal stress obtained theoretically is the same in all direction, in contrast to the anisotropic behaviours appeared in the 3D printed samples. This shows that the accuracy between the theoretical and the experimental test results is not ensured. Therefore, the analytical and computational methods can only be applied to estimate the tensile strength of 100%- filled specimens. But at this moment, these methods are not capable of predicting behaviour of a product printed in different settings.

5.2 Tensile Testing Analysis

5.2.1 Elastic Modulus

Table 8. *Difference in Yong's modulus between the practical test and the standard value*

Type of specimen	E_{exp} $[MPa]$	E_{exp}/E_{FEA}
1	608.046	0.184
2	674.994	0.2
3	605.54	0.183
4	636.212	0.192
5	727.1	0.22
6	632.62	0.191
7	932.21	0.28
8	628.807	0.19

9	563.816	0.17
10	749.866	0.227
11	852.083	0.258

The ratios of the experimental Young's modulus to the material's standard elastic modulus ($E_{FEA} = 3.3\ GPa$) are given in Table 8. The order of the specimen is the same as categorised in Table 3. By dividing the practical results to the standard modulus, the percentage differences of the Yong's modulus range between 17% to 28%. The author speculates the variation in the elastic property is attributed to two factors: atomic bonding and impurity in the filament. Firstly, greater bonding strength can increase the stiffness of the material and the energy to separate the atoms from one another. Comparing to a solid sample, the binding energy in a porous specimen is lower. Hence, the molecules also easily to slide on other when force is applied. As the stress required to produce a given strain decreases, the Yong's modulus also decreases. The second reason concerns the presence of impurity in the printing filament. Both the history of the filament and the testing conditions (the feedstock used, the way the test pieces were manufactured, etc.) for studying material properties are not provided. The printing filament may contain several reinforced materials and its properties of a 3D printed part may alter after being processed twice (when the filament was produced and when it is 3D printed). Therefore, this could explain why the experimental elastic modulus has lower value than the standard one.

5.2.2 Printing Orientation

It can be seen that the ZX-oriented (upright) sample possesses the lowest ultimate tensile strength as well as strain elongation, which has a magnitude of $18.98\ MPa$ and 3.66% respectively. The XY-oriented (flat) specimen failed at $22.158\ MPa$, which shows 1.45% reduction in tensile strength when compared with the XZ-oriented specimen, whose failure was at $22.484\ MPa$. However, the result for the elongation at break of the sample printed on the flat (XY) side was 14.6% larger than the one printed in XZ (edge) direction.

As previously stated, raster angle is one of the essential factors that has an impact on the final properties of the print. The considerable decrease in tensile strength of the ZX-oriented (edge) sample can be attributed to the perpendicular of each layer to the loading

direction. In other words, the upright specimens rupture at the point where the bond between layers fails, while more force is needed to break apart the filament in other two directions. Figure 13 presents the toolpath of the upright specimen generated by MakerBot having a raster angle of 90°. The XY-oriented (flat) sample was built on a 0° layer following a 90° layer, while the sample printed in on-edge direction was built with two 0° layers and one 90° layer. This explains why the tensile strength of the latter was slightly higher than the first one.

5.2.3 Infill and Layer Thickness

Several studies have proved that the increase of tensile strength and modulus were based on the following order of orientation: upright, flat and on-edge [47], while Smith et al. [48] research demonstrated the contrast, where they found XY-oriented (flat) sample possessed the highest strength. However, the higher in tensile strength and elastic modulus for on-edge direction compared to flat direction is only correct in a few cases in this work.

First of all, in terms of layer thickness, the author has anticipated that the decreasing in layer thickness of the print will lead to the increasing of tensile strength. But it can be seen from Figure 21.a that for the XY-flat orientation, the tensile strength was highest for the 0.5 mm specimen ($27.787\ MPa$) and lowest for the 0.2 mm specimen ($22.158\ MPa$), while on the contrary, the 0.1 mm-XZ-edge sample produced the highest strength ($23.13\ MPa$) and the 0.5 mm-XZ sample gave the lowest one ($21.535\ MPa$). The same chart also shows that the difference between the tensile strengths for the two directions of the same layer thickness is not significant as one of the two is slightly higher than the other, with the exception of the 0.5 mm layer thickness case. The exceptional high strength in this case could be due to the strong interlayer adhesion between layers that is explained in the next section.

Secondly, the ultimate tensile strength was recorded to significantly elevated when the infill level of the print reaches its maximum. This is due to the interior of the parts being filled up with more material, which required extra force to apply on the samples in order to break it apart. Figure 22.a shows an increase in infill from 10% to 50% and from 10% to 95% has enhanced the material strength to 30.5% and 85% for the XY-flat direction, respectively. In addition, for the XZ-edge orientation, the percentages were 34% and

74.7%. Both the strength of the XZ-oriented (on-edge) specimens with the infill of 20% and 50% were higher than the XY-flat direction. The results for these two on-edge samples were reported to be $24.573\ MPa$ and $30.18\ MPa$, indicating a difference of 8% and 4.34% in the strength value when comparing to the flat samples. Nonetheless, the trend did not continue to increase for the XZ-95% specimen. Its maximum strength slightly dropped and reached the value of $39.29\ MPa$, which is 4.3% lower than the value of the other orientation with the same infill.

Furthermore, strain at break was also determined. Looking at Figure 20, Figure 21.b and Figure 22.b, where printing orientations evidently had an impact on the fracture strain. The elongation at break, in every case, was shown highest for flat-oriented parts, following by the on-edge and upright orientation. However, it can be observed that there is no associated relation between the elongation at break with the tensile strength and modulus of elasticity. The increase in fracture strain does not result in lower strength or elastic modulus, and vice versa. Moreover, there seems to be a trend between the strain and the range of infill chosen. For both the XY-flat and XZ-edge direction, the increase in the mentioned setting parameter has raised the samples' elongation at break and samples with 95% infill produced the highest fracture strain. The ratio of the highest to the lowest strain for specimens in these two orientations was relatively closed, which is around 27%-28%. It is, however, impossible to control the material's properties during the printing process, especially with the technology of a commercial 3D printer. Hence, the printed objects are likely to behave anisotropically, which explains the non-linear connection among the tensile properties. Another theory that can be contributed to the lower strain of upright and on-edge specimens than of the flat ones is the way the samples were printed. The first ones were printed without support while the latter were generated vertically, weakening the bonds between the interlayers. As a result, this has limited the extension in length of the sample, causing the low elongation at break in the XZ (upright) and ZX (on-edge)-directed samples.

5.2.4 Correlations between Interlayer Bonding and Mechanical Strength

The cooling process, starting from the filament deposition phase to the interlayer adhesion state, from the nozzle temperature to the build plate and environment temperature, is one of the factors attributing to the product quality. The process includes five phases: Sinter

(1), Crystallization (2), Glass transition (3) and Shrinkage phrase (4+5) [56]. Sintering is a point when polymer chains from the deposited layer diffuse with the previous layer at the cross section by convection. Upon cooling, the material passes to the second phrase, crystallization, when the molecules in the polymer chains are tightly bonded. The high degree of crystallization indicates greater mechanical properties of a component. It is improved when the part has a longer cooling time. Next, the material's glass transition temperature is considered when it comes to the third state. It is important to keep the material above T_g as it increases flowing, avoiding voids created between layers. In addition, the part's dimensional accuracy can be reduced if flowing is not well controlled. Another reason that the temperature should not be lower than T_g is that the temperature distribution around the part is consistent, preventing the object from shrinking unsteadily. Residual stresses may accumulate when inconsistent shrinking occurs, which results in warping. [56] As PLA's T_g is around 60℃ and the bed temperature is always kept above this temperature, it is less likely to undergo warping. However, for materials with a high glass transition temperature, the parts probably undergo longer shrinking.

In this experiment, the cooling time of samples with different process parameters are evaluated. Out of three orientations, the flat samples are the only one that have unchanged deposited-layer shape throughout the whole printing process, showing that the temperature in the whole specimens are the most evenly distributed. Moreover, when looking at three samples in the beginning of the printing process, it can be seen that the flat one has the largest area per layer, which means it takes longer time to finish one layer and the material, thus, has more time to cool down and becomes more crystallized. These two features, as stated above, strengthen the flat specimen's tensile strength.

The bed and nozzle temperature are worth considered as well. These are two factors that directly influence how the interfacial bonds are formed and their quality [49]. High nozzle temperature re-melts the previous layer and by heat conduction, the intermolecular diffusion takes place, increasing the layer-to-layer coalescence. Furthermore, greater surface contact area can also improve the interlayer bonding as the voids generated between layers reduces when the temperature increases. Even though the bed temperature does not critically affect the interlayer adhesion, it keeps the print in the semisolid state and avoids

the deposited material cooling down too fast [49]. As a result, it improves the layer adhesion and this could be another reason why the quality of the flat specimens is strongest. As they have the least total number of layers and each layer is tightly fused and stays close to the print bed, unlike the other two directions, when the state of every layer is varied.

Lastly, layer thickness also has the correlation with the layer-to-layer adhesion. Low layer height results in faster cooling time and the build-up of residual stresses in the printed part. High layer height decreases the contact area, reflecting in the poor bonding strength. [49] However, the experimental results for this work are mixed. In terms of layer height, the 0.5 mm in layer thickness flat samples and the 0.1 mm in layer thickness on-edge specimens were recorded to have the highest strength.

5.3 Microscopy Imaging Analysis

Dark mode was applied while observing the samples. It can be perceived that the increase in layer thickness leads to the expand of the filament layers. Figure 24.a and 24.b also show that the filament fused together better when low layer thicknesses were chosen. The top surface of both samples was not significantly affected by the tensile loading and all the layers were still properly aligned. On the other hand, the 0.5 mm-specimen displays the gaps between each layer as it was not well merged into each other. These gaps tend to grow wider when subjecting to the pulling force from the tension test. The weak bond between layers of the 0.5 mm-samples and the almost empty interior structure (as the infill is only 10%) have made the parts easily break apart if more force is applied on them. Therefore, it is recommended that with any model printed in 0.5 mm- layer thickness, the infill should be increased to 50% or higher.

Figure 25 shows that pores between layers were detected on the cross-sectional surface of the flat and on-edge-specimens. Filament orientation can also be observed in these images. It can be seen that the number of pore increases along the edge of the cross section when the filament orientation matches the direction of the applied force. In addition, the pore size widens when the contact area between the deposited layers decrease. Infill pattern is also an element that directly affects several things such as micro-void formation,

void shape and volume fraction. All of these defects possibly lead to the alteration in the part's final mechanical properties. For the upright samples, the alignment of filament is found to be perpendicular to the loading orientation. Each layer is well bonded and the filament appears to have melted together. It is likely that the short time of finishing one layer and the insufficient time for curing have enhanced the fusion between layers.

6 CONCLUSION

In this work, the standard ISO test piece was designed and analysed both experimentally and theoretically. The components, made of PLA, were generated based on the chosen process parameters in the FDM manufacturing technique. The impact of the print settings particularly build orientation, on the tensile properties of the printed parts are evaluated. Optical microscopy study was carried out to examine the surface's microstructure. The main objectives of the thesis have been achieved.

The 3D model was simulated and analysed using FEA method. The maximum stress derived from this method showed a slight difference with the results calculated by the theoretical ways. The discrepancy between the theoretical and test results proves that the chosen methods used for the prediction of material strength are not reliable.

As expected, the ZX-upright samples have the lowest tensile properties out of the three orientations. In terms of the influence of layer thickness, there is no linear relation between the mentioned-parameter and the tensile strength. The experimental results show that the mechanical strength significantly elevated with an increase in infill density from 10% to 50% and 95%. Both the ultimate tensile strength of the 10% and 50%-filled on-edge samples are higher than the flat specimens but the trend is reversed for the 95%-filled parts. The strength values for parts printed in the XY-flat and XZ-on-edge orientation were reported to be quite close, except for the 0.5 mm in layer height case, where the percentage difference is 22.5%. Moreover, the strain at break was highest for every parts printed in XY direction.

The optical microscopy results suggest that the high layer thickness is not recommended as each layer is weakly bonded and there is space between filaments. This not only alters the final properties of the printed part, but also significantly affects its appearance. The observation of three samples printed in different directions shows that besides layer height infill density is a factor that leads to pore formation in the interior structure. However, another microstructural technique such as SEM could be adopted in order to obtain more detail information about the cause of failure of the material.

3D printing has become a potential technology and its applications have been expanded into several sectors. With a 3D printer, everyone is able to customise and produce their designs by themselves, which could reduce the cost of supply chain or packaging. Though more and more studies regarding the influence of print parameters on the quality of the final print have been conducted, the challenge of controlling the part's material properties during printing remains. In practice, the quality of a 3D product depends on a combination of factors from the designing stage until the printing stage, as well as materials and the type of printer used. Once these problems are tackled, 3D printing will become an indispensable tool in everyone's life and make a huge impact on the manufacturing industry.

REFERENCES

[1] Columbus, L. (2018) 'The State of 3D Printing, 2018', Forbes, 30 May. Available at: https://www.forbes.com/sites/louiscolumbus/2018/05/30/the-state-of-3d-printing-2018 [11 April 2019].

[2] Ayrilmis, N., Kariz, M., Kwon, J.H., Kuzman, M.K. (2019) 'Effect of printing layer thickness on water absorption and mechanical properties of 3D-printed wood/PLA composite materials', *Int J Adv Manuf Technol*, pp. 1-6. Available at: https://doi.org/10.1007/s00170-019-03299-9 [24 April 2019].

[3] Shubham, P., Sikidar, A. & Chand, T. (2016) 'The Influence of Layer Thickness on Mechanical Properties of the 3D Printed ABS Polymer by Fused Deposition Modeling', *Key Engineering Materials*, vol. 706, pp. 63-67. Available at: DOI: 10.4028/www.scientific.net/KEM.706.63 [24 April 2019].

[4] Yao, T., Deng, Z., Zhang, K. & Li, S. (2019) 'A method to predict the ultimate tensile strength of 3D printing polylactic acid (PLA) materials with different printing orientations', *Composites Part B*, pp. 393-402. Available at: https://doi.org/10.1016/j.compositesb.2019.01.025 [24 April 2019].

[4] Noorani, R. (2017) *3D Printing: Technology, Applications, and Selection*. Chapman and Hall/CRC.

[5] Goldberg, A. (2018) 'History of 3D Printing: It's Older Than You Are (That Is, If You're Under 30), *Redshift by Autodesk* ,13 April. Available at: https://www.autodesk.com/redshift/history-of-3d-printing/ [8 April 2019].

[6] West, J. & Kuk, G. (2016) 'The complementarity of openness: How MakerBot leveraged Thingiverse in 3D printing', *Technological Forecasting and Social Change*, vol. 102, pp.169-181. Available at: https://doi.org/10.1016/j.techfore.2015.07.025 [2 June 2019].

[7] Wohlers Associates (2014) 'Wohlers Report: 3D Printing and Additive Manufacturing, State of the Industry, Annual Worldwide Progress Report'. [2 June 2019].

[8] Bourell, D., Kruth, J.P., Leu, M., Levy, G., Rosen, D., M. Beese, A., Clare, A. (2017) 'Materials for additive manufacturing', *CIRP Annals – Manufacturing Technology*, vol. 66, no. 2, pp. 659-681. Available at: https://doi.org/10.1016/j.cirp.2017.05.009 [21 April 2019].

[9] Varotsis, A.B. (n.d.) 'Introduction to FDM 3D printing', *3D HUBS*. Available at: https://www.3dhubs.com/knowledge-base/introduction-fdm-3d-printing/ [18 April 2019].

[10] Satish Prakash, K., Nancharaih, T., Subba Rao, V.V. (2018) 'Additive Manufacturing Techniques in Manufacturing – An Overview', *Materials Today: Proceedings*, vol. 5, no. 2, pp. 3873-3882. Available at: https://doi.org/10.1016/j.matpr.2017.11.642 [18 April 2019].

[11] Redwood, B. (n.d.) 'Additive Manufacturing Technologies: An Overview', *3D HUBS*. Available at: https://www.3dhubs.com/knowledge-base/additive-manufacturing-technologies-overview [18 April 2019].

[12] Ooi, T. (2019) '5 Greatest 3D Printing Applications in 2019', *ALL3DP*, 4 February. Available at: https://all3dp.com/2/greatest-3d-printing-applications/ [11 April 2019].

[13] Dvir, T., Noor, N., Shapira, A., Edri, R., Gal, I., Wertheim, L. (2019)' 3D Printing of Personalized Thick and Perusable Cardiac Patches and Hearts', *Advanced Science*. Available at: https://doi.org/10.1002/advs.201900344 [11 April 2019].

[14] Redwood, B. (n.d.) 'Producing low-cost cast metal parts using 3D Printing', *3D HUBS*. Available at: https://www.3dhubs.com/knowledge-base/producing-low-cost-cast-metal-parts-using-3d-printing [11 April 2019].

[15] *A 3D printed house in Austin, Texas* (n.d.), image. Available at: https://computer.howstuffworks.com/3d-printed-houses-will-alleviate-homelessness.htm [11 April 2019].

[16] *The overview of the FDM process* (n.d.), image. Available at: https://thestempedia.com/tutorials/getting-started-with-3d-printing/ [9 April 2019].

[17] MANUFACTUR3D (2018) 'How FDM/FFF 3D Printing Technology Works?', *MANUFACTUR3D*, 29 January. Available at: https://manufactur3dmag.com/working-fdm-fff-3d-printing-technology/ [15 April 2019].

[18] Varotsis, A.B. (n.d.) 'Introduction to FDM 3D Printing', *3D HUBS*. Available at: https://www.3dhubs.com/knowledge-base/introduction-fdm-3d-printing [15 April 2019].

[19] Armstrong, C. (n.d.) 'Post processing for FDM printed parts', *3D HUBS*. Available at: https://www.3dhubs.com/knowledge-base/post-processing-fdm-printed-parts [15 April 2019].

[20] Cain, P. (n.d.) 'Selecting the optimal shell and infill parameters for FDM 3D Printing', *3D HUBS*. Available at: https://www.3dhubs.com/knowledge-base/selecting-optimal-shell-and-infill-parameters-fdm-3d-printing [17 April 2019].

[21] Li, N., Huang, S., Zhang, G., Qin, R., Liu, W., Xiong, H., Shi, G., Blackburn, J. (2019) 'Progress in additive manufacturing on new materials: A review', *Journal of Materials Science & Technology*, vol. 35, pp. 242-269. Available at: https://doi.org/10.1016/j.jmst.2018.09.002 [22 April 2019].

[22] Locker, A. (n.d.) '12 Vital Facts About Food Safe 3D Printing', *All3DP*. Available at: https://all3dp.com/1/food-safe-3d-printing-abs-pla-food-safe-filament/ [3 November 2019].

[23] 3D Printing Materials '3D Printing Materials', *3D PRINTING.COM.* Available at: https://3dprinting.com/materials/#filament [22 April 2019].

[24] Koslow, T. (2019) '2019 PLA Filament Guide – All You Need to Know', *All3DP*. Available at: https://all3dp.com/1/pla-filament-3d-printing/ [22 April 2019].

[25] Savioli Lopes, M., Jardini, A.L., Maciel Filho, R. (2012) 'Poly (Lactic Acid) Production for Tissue Engineering Applications, *Procedia Engineering*, vol. 42, pp. 1402-1413. Available at: https://doi.org/10.1016/j.proeng.2012.07.534 [24 April 2019].

[26] Gokhare, V.G., Raut, D.N., Shinde D.K. (2017) 'A review paper on 3D printing aspects and various processes used in the 3D printing', *Int J Eng Res Technol*, vol. 6, pp. 53-58. [24 April 2019].

[25] Hausman, K. & Horne, R. (2014) *3D Printing for Dummies*, John Wiley & Sons, Incorporated [24 April 2019].

[26] *Spools of PLA filaments* (n.d.), image. Available at: https://www.allthat3d.com/pla-filament/ [24 April 2019].

[27] Roylance, D. (2008) *Mechanical Properties of Material*.

[28] C. Hibbeler, R. (2018), 10th ed, *Mechanics of Materials*. Pearson Education, Inc.

[29] Ma, Y.Z., Sobernheim, D. & Garzon, J.R. (2016) 'Chapter 19 - Glossary for Unconventional Oil and Gas Resource Evaluation and Development', *Unconventional Oil and Gas Resource Handbook*, pp. 513-526. Available at: https://doi.org/10.1016/B978-0-12-802238-2.00019-5 [15 May 2019].

[30] Jones, D.R.H. & Ashby, M.F. (2019) 'Chapter 3 - Elastic Moduli', *Engineering Materials 1 (Fifth Edition)*, pp.31-47. Available at: https://doi.org/10.1016/B978-0-08-102051-7.00003-8 [15 May 2019].

[31] Licari, J.J. & Swanson, D.W. (2011) 'Chapter 7 - Test and Inspection Methods', *Adhesives Technology for Electronic Applications (Second Edition)*, pp. 345-377. Available at: https://doi.org/10.1016/B978-1-4377-7889-2.10007-5 [15 May 2019].

[32] *In-plane stress components of an element* (n.d.), image. Available at: https://www.efunda.com/formulae/solid_mechanics/mat_mechanics/calc_stress_transform.cfm

[33] *Mohr's Circle* (n.d.), image. Available at: Stress, Strain, and Structural Dynamics: An Interactive Handbook of Formulas, Solutions, and MATLAB Toolboxes.

[34] Makkonen-Craig, S. (2018), Topic 5 – Microscopy methods, lecture notes distributed in Material Analysis. Available at: https://arcada.itslearning.com [28 April 2019].

[35] Sawyer, L.C., Grubb D.T. & Meyers, G.F. (2008), *Polymer Microscopy*, Springer, New York. [28 April 2019].

[36] *Optical microscope* (2009), image. Available at: https://doi.org/10.1016/B978-0-12-394626-3.00009-0 [2 May 2019].

[37] Roane, T.M., Pepper, I.L. & Maier, R.M. (2009) 'Chapter 9 – Microscopic Techniques', *Environmental Microbiology (Second Edition)*, pp. 157-172. Available at: https://doi.org/10.1016/B978-0-12-370519-8.00009-2 [2 May 2019].

[38] *Transmitted light microscope & Reflective light microscope* (1993), image. Available at: Scanning and Transmission Electron Microscopy: An Introduction.

[39] Caprette, D.R. (2012) 'Light Microscopy', *Rice University*. Available at: https://www.ruf.rice.edu/~bioslabs/methods/microscopy/microscopy.html [2 May 2019].

[40] F. Mastro, P. (2016) *Plastics Product Design*. John Wiley & Sons, Incorporated.

[41] MakerBot 'PLA Material Large Spool'. Available at: https://store.makerbot.com/3d-printers/replicator-materials/pla-large/#truered

[42] Farbman, D. & D. McCoy, C. (2016) 'Materials Testing of 3D Printed ABS and PLA Samples to Guide Mechanical Design', *ASME 2016 11th International Manufacturing Science and Engineering Conference*. Available at: DOI: 10.1115/MSEC2016-8668 [2 June 2019].

[43] ISO 527-2, Plastics – Determination of tensile properties, 2012.

[44] Ahn, S.H., Montero, M., Odell, D., Roundy, S. & K. Wright, P. (2002) 'Anisotropic material properties of fused deposition modeling ABS', *Rapid Prototyping Journal*, vol. 8, no. 4, pp. 248-257. Available at: https://doi.org/10.1108/13552540210441166 [10 July 2017].

[45] Pic 10. Available at: https://airwolf3d.com/2018/03/20/material-strength-testing/

[46] Tulander, O. (2018) 'Polishing thin sections for analysis of 3D printed and injection moulded polymers', Bachelor thesis, Arcada. Available at: Theseus. [10 October 2019].

[47] Fayazbakhsh, K., Movahedi, M. & Kalman, J. (2019) 'The impact of defects on tensile properties of 3D printed parts manufactured by fused filament fabrication', *Materials Today Communications*, pp. 140-148. Available at: https://doi.org/10.1016/j.mtcomm.2018.12.003 [14 September 2019].

[48] Smith, W.C. & Dean, R.W. (2013) 'Structural characteristics of fused deposition modeling polycarbonate material', *Polymer Testing*, vol. 32, no. 8, pp. 1306-1312. Available at: https://doi.org/10.1016/j.polymertesting.2013.07.014 [14 September 2019].

[49] Aliheidari, N., Christ, J., Tripuraneni, R., Nadimpalli, S. & Ameli, A. (2018) 'Interlayer adhesion and fracture resistance of polymers printed through melt extrusion additive manufacturing process', *Materials & Design*, vol. 156, pp. 351-361. Available at: https://doi.org/10.1016/j.matdes.2018.07.001 [5 November 2019].

[50] Liu, Z., Zhang, M., Bhandari, B. & Wang, Y. (2017) '3D printing: Printing precision and application in food sector', *Trends in Food Science & Technology*, vol. 69, pp.83-94. Available at: https://doi.org/10.1016/j.tifs.2017.08.018 [21 November 2019].

[51] Wang, X., Zhao, L., Fuh, JYH. & Lee, HP. (2019) 'Effect of Porosity on Mechanical Properties of 3D Printed Polymers: Experiments and Micromechanical Modeling Based on X-ray Computed Tomography Analysis', *Polymers*, vol. 7. Available at: https://doi.org/10.3390/polym11071154 [26 November 2019].

[52] Siber, B. (n.d.) '3D Printing Infill Basics-Simply Explained, *ALL3DP.* Available at: https://all3dp.com/2/infill-3d-printing-what-it-means-and-how-to-use-it/ [26 November 2019].

[53] Mishra, P. (2017) 'What is Stress Concentration – Definition, Causes, effects and Prevention?', *Mechanical Booster*. Available at: https://www.mechanicalbooster.com/2017/04/what-is-stress-concentration.html [4 November 2019].

[54] COMSOL (2017) 'Finite Element Analysis (FEA) Software'. Available at: https://www.comsol.com/multiphysics/fea-software [4 November 2019].

[55] COMSOL (2017) 'Finite Element Mesh Refinement'. Available at: https://www.comsol.com/multiphysics/mesh-refinement [4 November 2019].

[56] Bähr, F. & Westkämper, E. (2018) ‘Correlations between Influencing Parameters and Quality Properties of Components Produced by Fused Deposition Modeling’, *ScienceDirect*, pp. 1214-1219. Available at: https://doi.org/10.1016/j.procir.2018.03.048 [5 November 2019].